Technology Collaboration Programme
by iea

International Energy Agency
Photovoltaic Power Systems Programme

Task 15 Enabling Framework for the Development of BIPV

PVPS

JOURNAL ARTICLE

Energy & Buildings

Multi-objective Assessment of BIPV Yield, Complementarity, and Economic Feasibility

August 2026

What is IEA PVPS TCP?

The International Energy Agency (IEA), founded in 1974, is an autonomous body within the framework of the Organisation for Economic Cooperation and Development (OECD). The Technology Collaboration Programme (TCP) was created with the belief that the future of energy security and sustainability starts with global collaboration. The programme is made up of 6.000 experts across government, academia, and industry dedicated to advancing common research and the application of specific energy technologies.

The IEA Photovoltaic Power Systems Programme (IEA PVPS) is one of the TCPs within the IEA and was established in 1993. The mission of the programme is to “enhance the international collaborative efforts which facilitate the role of photovoltaic solar energy as a cornerstone in the transition to sustainable energy systems”. In order to achieve this, the programme’s participants have undertaken a variety of joint research projects in Photovoltaic (PV) power systems applications. The overall programme is headed by an Executive Committee, comprised of one delegate from each country or organisation member, which designates distinct ‘Tasks’ that may be research projects or activity areas.

The IEA PVPS participating countries are Australia, Austria, Belgium, Canada, China, Denmark, Finland, France, Germany, India, Israel, Italy, Japan, Korea, Lithuania, Malaysia, Morocco, the Netherlands, Norway, Portugal, South Africa, Spain, Sweden, Switzerland, Thailand, Türkiye, the United Kingdom and the United States of America. The European Commission, Solar Power Europe and the Solar Energy Research Institute of Singapore are also members.

Visit us at: www.iea-pvps.org

What is IEA PVPS Task 15?

The objective of Task 15 of the IEA Photovoltaic Power Systems Programme is to create an enabling framework to accelerate the penetration of Building-Integrated Photovoltaics (BIPV) products in the global market of renewables, resulting in an equal playing field for BIPV products, Building-Applied Photovoltaics (BAPV) products and regular building envelope components, respecting especially economic, technological, legal, aesthetic, reliability and normative issues.

SUGGESTED CITATION

Yang, R. J., Liu, C., Sachchithananthan, M., Weerasinghe, N., Zang, Y., Wilson, H. R., Leloux, J., Valencia-Caballero, D., Zomer, C. D., Unger, M., Frontini, F., Ishii, H., Jayasuriya, S., Zhao, H., Leow, S. W., Liu, R., Vega de Seoane, J. M., Kim, J.-T., Macé, P., Anumba C.J., Zhao Y., Taylor, M. (2026). Multi-objective assessment of BIPV yield, complementarity, and economic feasibility. *Energy and Buildings, Vol. 369 Part B* (2026), 118031. https://doi.org/10.1016/j.enbuild.2026.118031

COVER PICTURE

BIPV skylight (photo: Mauro Gregori).

INTERNATIONAL ENERGY AGENCY

PHOTOVOLTAIC POWER SYSTEMS PROGRAMME

Multi-objective Assessment of BIPV Yield, Complementarity, and Economic Feasibility

IEA PVPS
Task 15
Enabling Framework for the Development of BIPV

Energy and Buildings,
Vol. 369, Part B,
DOI: 10.1016/j.enbuild.2026.118031

August – 2026

Energy & Buildings 369 (2026) 118031

Contents lists available at ScienceDirect

Energy & Buildings

journal homepage: www.elsevier.com/locate/enb

Multi-objective assessment of BIPV yield, complementarity, and economic feasibility

Rebecca Jing Yang [a,*], Chengyang Liu [b], Mathanky Sachchithananthan [b], Nilmini Weerasinghe [c], Yukun Zang [b], Helen Rose Wilson [d], Jonathan Leloux [e], Daniel Valencia-Caballero [f], Clarissa Debiazi Zomer [g], Malin Unger [h], Francesco Frontini [i], Hisashi Ishii [j], Sajani Jayasuriya [b], Hongying Zhao [b], Shin Woei Leow [k], Rui Liu [l], Jose M. Vega de Seoane [m], Jun-Tae Kim [n], Philippe Macé [m], Chinemelu J. Anumba [l], Yusen Zhao [b], Michael Taylor [o]

[a] *Department of Infrastructure Engineering, University of Melbourne, Melbourne, Australia*
[b] *School of Property, Construction and Project Management, RMIT University, Melbourne, Australia*
[c] *School of Engineering, RMIT University, Melbourne, Australia*
[d] *Fraunhofer Institute for Solar Energy Systems, Freiburg, Germany*
[e] *LuciSun, Rue Saint-Jean 29, 1495 Villers-la-Ville, Belgium*
[f] *TECNALIA, Basque Research and Technology Alliance (BRTA), Paseo Mikeletegi 2, San Sebastián 20009, Spain*
[g] *Universidade Federal de Santa Catarina/UFSC, Campus Universitário Trindade, 88040-900 Florianópolis, SC, Brazil*
[h] *RISE Research Institutes, Sweden*
[i] *University of Applied Science and Arts of Southern Switzerland (SUPSI), Mendrisio, Switzerland*
[j] *LIXIL Corporation, LIXIL Housing Technology, Technology Research Institute, 4-13-14, Higashi Shinagawa, Shinagawa City, Tokyo, Japan*
[k] *Singfilm Solar PTE LTD, Singapore*
[l] *M.E. Rinker, Sr. School of Construction Management, University of Florida, 573 Newell Dr, Gainesville, FL 32603, United States*
[m] *Becquerel Institute España, Spain*
[n] *Department of Architectural Engineering, Kongju National University, Shinwangdong 182, Kongju city, Chungnam, Republic of Korea*
[o] *EME Consulting LTD, United States*

ARTICLE INFO

Keywords:
Building-integrated photovoltaics (BIPV)
Economic viability
Energy yield
Multi-objective optimization
Smoothness
Temporal complementarity

ABSTRACT

Building-integrated photovoltaics (BIPV) are essential for the transition towards net-zero energy buildings, yet a comprehensive multi-regional understanding of how energy yield, temporal complementarity, and economic feasibility interact across diverse configurations remains limited. Task 15 of the International Energy Agency Photovoltaic Power Systems Programme conducted a cross-regional, multi-objective assessment of 357 BIPV design options across eight application types in 44 cities, using a standardized 1 m^2 module with efficiencies between 5% and 25%. Energy yields were simulated using climate-specific irradiance datasets, and economic viability was assessed under three price tiers. A multi-objective Genetic Algorithm optimized the azimuths of vertical BIPV based on temporal complementarity and smoothness of the aggregated generation profile with optimal-yield rooftop BIPV system and conventional PV system (BIPV-PV). The combination of rooftop and vertical BIPV demonstrates strong daily and seasonal complementarity, enhancing the stability and continuity of solar energy conversion across time scales. Complementary area-ratio analysis indicates that vertical BIPV surfaces require approximately 1.7–2.5 times more area to match the yield of optimally tilted rooftop BIPV-PV

Abbreviations: AC, Alternating Current; AOI, Angle of Incidence; API, Application Programming Interface; BAPV, Building-Attached Photovoltaics; BIPV, Building-Integrated Photovoltaics; CC, Capital Cost; DC, Direct Current; DHI, Diffuse Horizontal Irradiance; DNI, Direct Normal Irradiance; DSF, Double-Skin Façade; EBS, Electricity Bill Savings; FIT, Feed-in Tariff; GA, Genetic Algorithms; GHI, Global Horizontal Irradiance; GSA, Global Sensitivity Analysis; GS, Grid Savings; IEA, International Energy Agency; IEA-PVPS, International Energy Agency Photovoltaic Power Systems Programme; IEC, International Electrotechnical Commission; IRC, Inverter Replacement Cost; LCOE, Levelized Cost of Electricity; LMC, Lifecycle Maintenance Cost; MATLAB, Matrix Laboratory; MRV, Material Replacement Cost; NPV, Net Present Value; NSRDB, National Solar Radiation Database; NREL, National Renewable Energy Laboratory; POA, Plane of Array; PV, Photovoltaics; R&D, Research and Development; RE, Rebate; SALib, Sensitivity Analysis Library; SAPM, Sandia PV Array Performance Model; SC, System Capacity; STC, Standard Test Conditions; SV, Salvage Value; TMY, Typical Meteorological Year; USD, United States Dollars.

* Corresponding Author.
E-mail address: jing.yang.5@unimelb.edu.au (R.J. Yang).

https://doi.org/10.1016/j.enbuild.2026.118031
Received 1 December 2025; Received in revised form 12 July 2026; Accepted 29 July 2026
Available online 1 August 2026

systems. At low BIPV prices, over 90% of configurations become economically viable for efficiencies starting at around 18%, and in some cases even lower. Even at high price ranges, more than half remain viable, highlighting BIPV's increasing competitiveness and cost-reduction potential through improved installation practices and knowledge sharing. Overall, BIPV economic performance depends on complex, interdependent factors, indicating that single measures such as product cost-reduction are insufficient without holistic financial and market integration.

1. Introduction

Building-integrated photovoltaics (BIPV) replaces conventional building materials, serving a dual role as electricity generators and functional building elements [1]. Unlike the typical building-attached PV (BAPV) installation (roof-mounted), which exhibits peak generation around midday [2], BIPV yield a broader generation profile due to its range of orientations and tilt angles as a function of building surface exposition, as well as capturing reflected direct and diffuse radiation from nearby surfaces, even in shaded or dense urban areas [3]. BIPV replicates the role of a power plant at building scale, that potentially can be integrated into the entire building envelope [4]. BIPV is often compared to BAPV and to conventional building materials in terms of electricity generation and economic viability [5,6]. Achieving optimal energy yield alongside positive economic performance is key for social acceptance and is influenced by multiple factors [7].

For the past decades, research field of BIPV is gradually leaning from material and technological advancement towards the optimisations of field trails, performance evaluation, and technoeconomic assessments [8]. For instance, a study for BIPV adoption in office building in five Chinese cities [9] considering relevant factors of building orientations, access to visual light, PV material, etc. The authors identified that among the analysed parameters, the deployment orientation is of the greatest significance for BIPV energy and economic performance across the cities. A recent study for BIPV economic viability for India [10] revealed the similar observation that the angular settings for BIPV system have strong impacts on the economic outlook. This study selected temperature-corrected efficiency as the method for BIPV performance evaluation and key economic performance indicators of NPV, LCOE, and payback year. A study in Scottland [11] adopted similar approach across four Scottish urban area. The study formed a workflow with PVsyst for PV performance modelling and MATLAB for automated analytic process. Notably, this study applied a single optimal angular setting across all studied location while arguing that the angular placements are crucial for the analysed economic indicators including yield generation per year, LCOE, and payback years.

The recent studies as discussed above shown that the BIPV systems can achieve excellent economic and energy performance locally, while most of these studies emphasized the importance of the designs of implementation in achieving expected performance, especially the angular settings. Yet, it is evident that the current studies are usually limited to geographic locations [10,12,13], case studies on individual buildings [14,15], limited angular settings [11], and pre-selected BIPV products. Although these refined scopes allow more sophisticated performance modelling and specific considerations for local climatic, economic, and product-specific parameters settings, it is often lack of grounds to provide generic findings to advise the BIPV implementation as an effective measure to facilitate renewable energy transition in the built environment. This leads to fragmented knowledge that is difficult to generalize. In the absence of cross-regional comparative studies, assessments of BIPV applications remain highly case-specific, limiting their relevance for broader market adoption, policy formulation, design strategy development and early investment decision-making.

In relation to algorithmic development for BIPV design optimisation, a substantial body of literature has investigated various approaches, including metaheuristic-based multi-objective optimisation [9,15–17], mathematical optimisation methods for identifying global optima through the construction of response surfaces [11], and integrated machine-learning approaches [16,18]. The purpose of this review is not to critique the advancement of optimisation algorithms, as this is beyond the scope of the present study. Rather, it is to contextualise the selection of optimisation strategies commonly adopted in BIPV-related studies. Mathematical optimisation methods can be effective for well-structured or relatively linear problems but may become less flexible when the design space involves multiple interacting parameters and non-linear constraints. Machine-learning-based approaches can provide highly refined predictive or optimisation capabilities, but often require extensive training data, careful tuning, and may involve reduced interpretability or increased computational burden. In comparison, metaheuristic approaches, such as particle swarm optimisation and genetic algorithms, offer a practical balance between search capability, computational demand, and implementation flexibility, making them suitable for complex BIPV design optimisation problems where multiple objectives and constraints must be considered simultaneously.

Built upon the existing knowledge development in the field of BIPV and the identified research gaps, this study conducts a macro-level, multi-objective assessment of BIPV energy yield, temporal complementarity and economic feasibility, using standardized 1 m^2 modules with module efficiencies ranging from 5% to 25% in 1% increments. Conducted as a part of the International Energy Agency Photovoltaic Power Systems Programme (IEA-PVPS) Task15, the analysis covers eight BIPV applications across 44 cities in 12 countries (see Table 1).

Following objectives are proposed for this study: (1) To identify viable design options for BIPV systems across various climate zones; (2) To conduct energy-yield simulation and multi-objective optimization/trade-offs across energy generation and stability indicators; (3) To evaluate the techno-economic feasibility of BIPV systems following IEA-PVPS framework. Associated with the identified objectives, the key contribution of this study are presented as the followings: (1) the construction of a 44-city comparative BIPV economic assessment; (2) the integration of expert-informed local economic parameters into a harmonised simulation framework; and (3) the identification of cross-city and cross-economy patterns in BIPV economic performance that are not visible from single-city or case-specific studies.

The remainder of this paper is structured as follows: Section 2 describes the materials and methods used in this study. Section 3 presents and discusses the combined results. Section 4 concludes the study by summarizing key insights and implications.

2. Materials and methods

The diagram above (Fig. 1) demonstrates the design and workflow of this study. The workflow provides a macro-level assessment covering 44 cities with diverse climatic conditions and irradiance profiles focusing on BIPV's energy yield capacity, complementarity effect to smooth the generation pattern, and provide broader insights into the techno-economic feasibility of the BIPV applications across different climate zones. Detailed data collection and methods are introduced in the following sections.

2.1. BIPV configuration design

2.1.1. Selection of cities

The selected cities across six continents represent a broad spectrum of climatic conditions and solar irradiance levels, enabling evaluation of BIPV performance potential under varying environmental conditions. A standardized 1 m^2 BIPV surface area is used across all locations to ensure comparability. The study covers 44 cities in 12 countries, representing major climate zones relevant to the built environment. Global horizontal irradiance (GHI) values are used to ensure the inclusion of cities with both high and low solar energy potential. Summary of selected cities, their GHI values [19], and corresponding climate zones [20] is presented in Table 1.

2.1.2. Angular configurations of BIPV

Seventeen distinct configurations identified by an "Option coding" are considered based on: the tilt and azimuth angle of the BIPV panels. The tilt angles included horizontal (tilt angle of 0°), optimal (optimized local tilt angle that achieves highest annual plane of array (POA) irradiation), latitude (tilt angle, same as the absolute value of local latitude), 75° (tilt angle of 75° inclination from horizontal) and 90° (vertical). Each tilt angle, except "Horizontal", has four corresponding azimuth orientations: north (0°), east (90°), south (180°), and west (270°).

The selection of tilt angles includes practical configurations such as the annual-yield-optimized tilt angle, the empirical practice of using local latitude as the tilt angle [21], and typical façade tilt angles of 75° and 90° for envelope-integrated BIPV, as outlined by IEC 63092–1:2020 [22]. In addition, the 0° tilt angle was included to represent near-horizontal BIPV applications associated with specific building elements, such as flat or continuous roofs, skylights, and selected external integrated devices. This selection is further supported by [23], which identifies BIPV as part of building-envelope systems including continuous roofs, atrium/skylight systems, façades, and external integrated devices.

Table 2 summarises these systematic breakdowns of tilt and orientation angles for different BIPV applications in the simulation. A checkmark indicates that the specific tilt and azimuth combination is suitable or applicable for the corresponding BIPV application and is used as a scenario in the simulation.

These angular configurations are then analysed in combination with 21 nameplate module efficiency levels, ranging from 5% to 25% at 1% increments. This resulted in a total of 357 design options (17 angular configurations × 21 efficiencies).

2.1.3. Selection of applications

The BIPV application types are classified based on the standardized definitions from the IEA-PVPS Task 15 report on BIPV application typologies [23]. These classifications are based on BIPV integration into specific elements of the building envelope, aligning with traditional construction system definitions. The main categories are roofs: discontinuous roof, continuous roofs and skylights, façade: curtain walls, rainscreens, double-skin façade (DSF), external integrated devices:

Table 1
Climatic details of the selected cities.

No.	Continent	Country	Country Code	City	GHI	Climate zone
1	Asia	China	CHN	Chengdu	900	Warm temperate moist
2	Asia	China	CHN	Beijing	1400	Warm temperate dry
3	Asia	China	CHN	Xining	1700	Boreal dry
4	Asia	China	CHN	Shenyang	1400	Humid continental dry
5	Asia	China	CHN	Guangzhou	1500	Humid subtropical
6	Asia	China	CHN	Shanghai	1500	Humid subtropical
7	Asia	Japan	JPN	Aomori	1204	Cool temperate moist
8	Asia	Japan	JPN	Tokyo	1423	Warm temperate moist
9	Asia	Japan	JPN	Fukuoka	1350	Warm temperate moist
10	Asia	South Korea	KOR	Seoul	1400	Warm
11	Asia	South Korea	KOR	Daejeon	1500	Temperate
12	Asia	South Korea	KOR	Gwangju	1450	Dry
13	Asia	South Korea	KOR	Busan	1550	Humid subtropical
14	Asia	Singapore	SGP	Singapore	1600	Tropical moist
15	Asia	Indonesia	IDN	Jakarta	1400	Tropical moist
16	Asia	Indonesia	IDN	Medan	1700	Tropical moist
17	Africa	Nigeria	NGA	Port Harcourt	1500	Tropical moist
18	Africa	Nigeria	NGA	Abuja	1800	Subtropical moist
19	Africa	Nigeria	NGA	Kaduna	2000	Subtropical moist
20	Africa	Nigeria	NGA	Kano	2150	Tropical dry
21	North America	Canada	CAN	Toronto	1200	Humid continental, hot summer
22	North America	Canada	CAN	Winnipeg	1400	Humid Continental, warm summer
23	North America	Canada	CAN	St. Johns	1000	Humid continental, warm summer
24	North America	Canada	CAN	Yellowknife	1100	Subarctic
25	North America	USA	USA	Portland	1300	Cool temperature moist
26	North America	USA	USA	Denver	1700	Cool temperature dry
27	North America	USA	USA	Atlanta	1800	Warm temperate moist
28	North America	USA	USA	Albuquerque	2100	Warm temperate dry
29	North America	USA	USA	Phoenix	2200	Subtropical dry
30	South America	Brazil	BRA	Curitiba	1500	Cool temperature moist
31	South America	Brazil	BRA	Rio de Janeiro	1700	Subtropical moist
32	South America	Brazil	BRA	Cuiaba	1900	Tropical moist
33	South America	Brazil	BRA	Teresina	2100	Tropical dry
34	Europe	Spain	ESP	Gijon	1269	Oceanic
35	Europe	Spain	ESP	Madrid	1790	Continental Mediterranean
36	Europe	Spain	ESP	Malaga	1862	Hot-summer Mediterranean
37	Europe	Sweden	SWE	Stockholm	989	Cool temperate moist
38	Europe	Sweden	SWE	Lund	1028	Cool temperate moist
39	Europe	Sweden	SWE	Kiruna	803	Boreal moist
40	Australasia	Australia	AUS	Melbourne	1500	Cool temperate moist
41	Australasia	Australia	AUS	Rockhampton	1800	Humid subtropical
42	Australasia	Australia	AUS	Wagga Wagga	1500	Humid subtropical with semi-arid influence
43	Australasia	Australia	AUS	Adelaide	1700	Mediterranean, hot summer
44	Australasia	Australia	AUS	Broome	2000	Subtropical steppe (semi-arid)

balcony balustrades and solar shading devices: shading device. This classification highlights the dual role of BIPV as both a building envelope component and a source of renewable energy, emphasizing its integration into architectural and structural functions.

2.2. Energy assessment

2.2.1. Model components and functional description

Hourly weather data and site-specific information are used to estimate the energy performance of the systems following the sequential workflow illustrated in Fig. 2. The simulation first determines the solar position based on the geographic location and timestamp. The calculated solar position together with irradiance data is then used to estimate the plane of array (POA) irradiance incident on the receiving surface. Subsequently, PV cell temperature is calculated and incorporated into a temperature-adjusted efficiency to estimate the DC power output. Finally, the NREL inverter model is applied to convert the DC output into AC energy generation.

Table 3 summarises the data inputs and system parameters used in the energy simulation. These inputs directly drive the sequential modelling workflow described above, where meteorological variables are used to determine solar geometry, while system parameters define the conversion from incident solar energy to electrical output.

2.2.1.1. Solar position and plane of array (POA) irradiance. The solar position is estimated using Sandia National Lab's ephemeris function. The function takes the input parameters for the local time in the format of YYYY-MM-DD-HH-mm-ss, geographic location (latitude, longitude, and altitude), atmospheric pressure in Pascals (default to 1 ATM), and the ambient air temperature (°C). The function output includes the sun's azimuth angle (°), actual elevation (°), apparent elevation (angle of the sun above the horizon after accounting for atmospheric refraction), and the solar time in decimal hours with 12.00 corresponding to solar noon. The outputs from the solar position function (solar zenith angle and solar azimuth angle) together with PV module tilt angle (°) and azimuth angle (°) are used as inputs to PVLib's AOI function. This resulted in angle of incidence (AOI) (°) under the defined solar position/module angular conditions.

The calculated AOI is then used to determine the irradiance incident on the tilted PV surface. The direct irradiance is calculated as the product of DNI and the cosine of AOI. The computation only considered when the sun is above the receiving plane corresponding to the sun elevation angle is larger than 0° and AOI values are between 0° and 90°. The diffuse irradiance is calculated using the Hay and Davies model [25,26]. This model takes DHI and the tilt angle of the receiving surface as inputs and estimates the diffuse irradiance on the tilted plane. Ground-reflected irradiance is calculated using PVLib's ground diffuse reflection function. This required inputs of GHI, the receiving surface's tilt angle, and the ground reflection coefficient (albedo). A default albedo value of 0.2 is used in this study.

The POA irradiance on the tilted PV surface is obtained from the combination of direct, diffuse sky, and ground-reflected irradiance components, with the direct component adjusted using the AOI. The resulting POA irradiance therefore represents the total solar energy

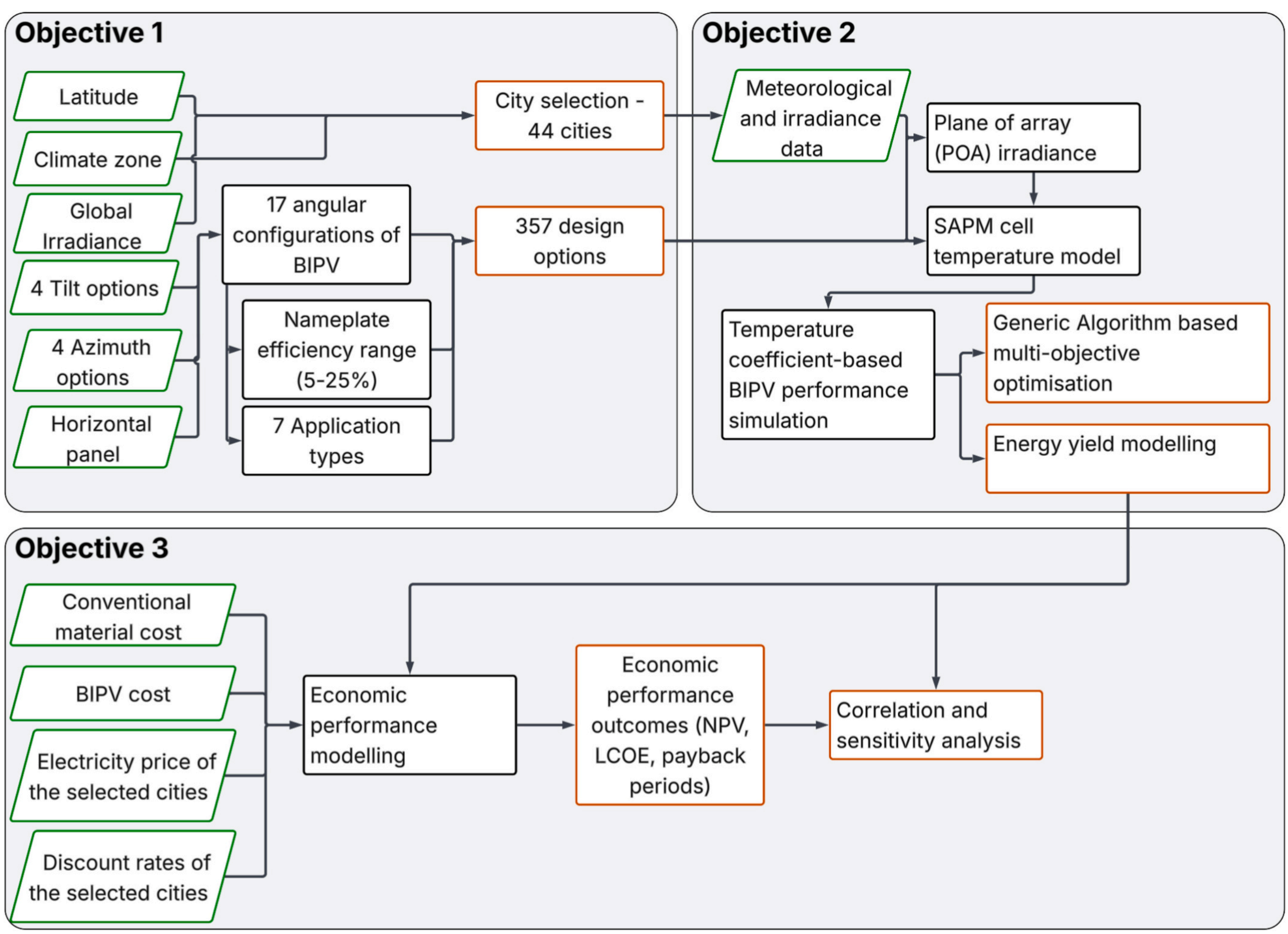

Fig. 1. Study design and workflow.

Table 2
Angular configurations of different BIPV application.

Config-uration coding	Tilt	Azimuth	Roof BIPV			Façade BIPV			
			Continuous roof	Discontin-uous roof	Skylight	Balustrade	Curtain wall	Rain-screen	Shading device
1	0° (Horizontal)	N/A	✔	✔	✔				✔
2	Optimal	0° (N)	✔	✔	✔				✔
3	Optimal	90° (E)	✔	✔	✔				✔
4	Optimal	180° (S)	✔	✔	✔				✔
5	Optimal	270° (W)	✔	✔	✔				✔
6	Latitude	0° (N)	✔	✔	✔				✔
7	Latitude	90° (E)	✔	✔	✔				✔
8	Latitude	180° (S)	✔	✔	✔				✔
9	Latitude	270° (W)	✔	✔	✔				✔
10	75°	0° (N)				✔	✔	✔	✔
11	75°	90° (E)				✔	✔	✔	✔
12	75°	180° (S)				✔	✔	✔	✔
13	75°	270° (W)				✔	✔	✔	✔
14	90°	0° (N)				✔	✔	✔	✔
15	90°	90° (E)				✔	✔	✔	✔
16	90°	180° (S)				✔	✔	✔	✔
17	90°	270° (W)				✔	✔	✔	✔

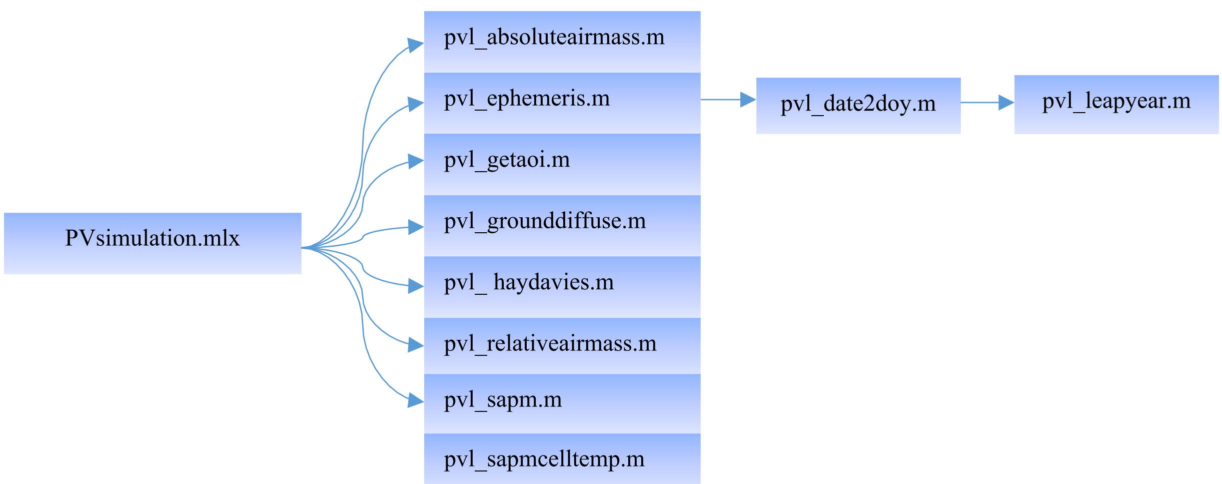

Fig. 2. Dependency diagram illustrating the overall workflow and function relationships within the simulation model [24].

Table 3
Data inputs for energy simulation.

Data categories	Input parameter	Data structure	Unit	Reference value	Data source
Time series	Direct Normal Irradiance (DNI)	Time series	W/m^2	NA	Primary data source: NREL National Solar Radiation Database (NSRDB) API
	Diffuse Horizontal Irradiance (DHI)	Time series	W/m^2	NA	
	Dry bulb temperature	Time series	°C	NA	Secondary data source: EnergyPlus TMY hourly weather data base
	Wind speed	Time series	m/s	NA	
System specification	DC/AC ratio	Constant		1.2	
	Inverter efficiency	Constant	%	96	
	Module area size	Constant	m^2	1	
	Module STC efficiency	Variable	%	5–25	
	System loss ratio	Constant	%	20	

incident on the PV surface and is used as the primary input for subsequent performance modelling.

2.2.1.2. Cell temperature and electrical performance. The POA irradiance together with wind-speed (m/s), and ambient air temperature (°C) is used as inputs to estimate PV cell temperature using Sandia PV Array Performance Model (SAPM) cell temperature function [27]. It characterizes PV module behaviour using five points on the IV curve: short circuit current (Isc, 0), current with ½ open circuit voltage (Ix, ½ Voc), current and voltage at maximum power (Imp, Vmp), current with ½ of the aggregated open circuit volage and maximum power voltage (Ixx, ½ (Vmp + Voc), and open circuit voltage (0, Voc).

Although the SAPM approach offers a reasonably accurate representation of PV operational performance, its reliance on field-measured coefficient sets introduces additional uncertainties when applied to present study. To balance model fidelity, transparency, and applicability across diverse case studies, this study adopts a hybrid modelling approach. The cell temperature (T_c) is calculated using the established thermal framework from the SAPM, ensuring that key physical drivers such as irradiance, ambient temperature, and wind effects are retained. However, instead of resolving the full I—V curve, the electrical performance is approximated using a temperature-corrected efficiency [28] formulation defined using eq. (1).

$$\eta = \eta_{ref} \times \left(1 - \mu\left(T_c - T_{ref}\right)\right) \quad (1)$$

where, $\eta_{ref}$is the system reference efficiency (%) provided by the manufacturer, μ is the temperature coefficient (1/K) measured and provided by the manufacturer and $T_{ref}$is the reference temperature (°C) at which reference efficiency is tested. Default values are selected for the temperature coefficient and reference temperature, which are −0.005 for μ, and 25 °C for T_{ref}.

This simplification is motivated by two key considerations. First, the detailed parameterization required for full SAPM implementation (e.g., spectral and I—V curve coefficients) is not consistently available for contemporary BIPV products, limiting model applicability and reproducibility. Second, for large-scale comparative analyses across multiple climates and product types, the marginal gain in accuracy from full I—V modelling is outweighed by increased data requirements and associated uncertainties.

By leveraging SAPM-derived cell temperature while simplifying the electrical model, this approach preserves the dominant thermal-performance coupling while enabling consistent, transparent, and scalable evaluation across all study cases. Similar trade-offs between accurate physical models and thermal coefficient models have been discussed in many previous studies. In a study of [29] compared a simplified model with the detailed model chain of single-diode and SAPM model. The authors suggested that despite the complete model chain having significant advantages for low absolute errors, the simplified model exhibits stronger robustness across diverse climatic and temporal conditions. It is also suggested by IEA-PVPS Task 13 [30] that the selection of PV model depends on the reason for modelling, and it is applicable to use efficiency-only model when the purpose is to calculate simple kWh/kWp. Yet it should be noted that complete and accurate model chains that PV modules' I-V characteristics are still the more suitable evaluation approach, especially for studies with scope of specific sites and/or specific systems.

Therefore, an approximation of the BIPV system's operating power can be defined by eq. (2).

$$P_{DC} = POA \times \eta \times S \quad (2)$$

where P_{DC} is the DC output power (W) of the BIPV system, and S is the size of the PV module (m^2).

The NREL inverter model is then used to convert the DC power output into AC power output. The model estimates the AC output of the PV model by assuming a reference inverter efficiency of 0.9637 (η_{ref}). As this study applies scenario analysis using multiple PV modules with various nameplate capacity, it is unreasonable to set a default inverter capacity for all these modules. Hence, an assumption has been made that the inverter AC capacity meets the upper limit of the PV module's nameplate DC output. With a further assumption of 1.2 DC-to-AC ratio, the assumed inverter AC capacity for each module can be calculated using eq. (3).

$$P_{inv_{AC}} = P_{nameplate\_PV_{DC}} / R_{DC-AC} \quad (3)$$

The default efficiency of the inverter is set to 96% for all modules, and the AC power outputs can be estimated using the eqs. (4), (5) and (6) [31].

$$P_{inv_{DC}} = \frac{P_{inv_{AC}}}{\eta_{defaultEfficiency}} \quad (4)$$

$$\eta_{inv} = \frac{\eta_{defaultEfficiency}}{\eta_{ref}} + 0.9858 - 0.0162 \times F_{load} - \frac{0.0059}{F_{load}} \quad (5)$$

$$P_{AC} = P_{DC} \times \eta_{inv} \quad (6)$$

2.2.2. Energy simulation

This section extends the modelling approach described in the section 2.2.1 to system analysis across the selected cities. The hourly AC power outputs obtained from the simulation model are used to evaluate optimal design configurations, temporal performance characteristics and spatial variations in BIPV system performance.

For each city, a bounded one-dimensional optimisation is implemented in MATLAB to identify the annual-yield-maximising tilt angle under four fixed azimuth orientations: 0°, 90°, 180°, and 270°. The tilt angle is treated as the decision variable, and the objective function for this process is formulated as the negative annual energy yield calculated from location-specific weather data, allowing MATLAB's fminbnd function to identify the tilt angle associated with the maximum annual generation within the defined angular range.

The process begins by iterating over a list of cities. For each city, the algorithm loads relevant weather data and then applies fminbnd to determine the optimal tilt angle corresponding to each of the four cardinal azimuths of each city. Further methodological details are provided in Supplementary Material S1. The resulting optimal tilt angles for each azimuth and city are reported in Supplementary Table 1.

Using the optimized configurations, hourly AC power output profiles are generated for each city to evaluate the impact of varying tilt and azimuth configurations on BIPV performance. The power output for each hour represents the average output over all days of the month at that specific hour (e.g., the value at 7:00 AM is the average of daily outputs at 7:00 AM across the month).

These hourly values are plotted in time-series line charts, with the x-axis spanning from 00:00 to 23:00 to reflect a full day of output variation across months. As illustrated in Fig. 3, the x-axis chronicles the time from 0:00 to 23:00 in hourly intervals. The power output for a given hour represents the average of the aggregated power outputs at that time over the month duration (e.g., the combined output at 7:00 AM from February 1st to 28th, subsequently averaged).

To further understand the benefits of vertical BIPV (i.e. 90° tilt) annual average daily generation profiles of optimally tilted, equator-facing rooftop BIPV-PV and vertical BIPV are compared. Both rooftop BIPV-PV and vertical BIPV configurations are modelled with a nameplate efficiency of 20%.

2.2.3. Coupling and optimization

To investigate the coupling effects between optimal-yield rooftop BIPV-PV and vertical BIPV, three PV configurations are simulated for each of the 44 selected cities. These include (i) optimal-yield rooftop BIPV-PV: A unit size rooftop BIPV or PV system facing the equator and with an optimized tilt angle as outlined in section 2.2.2, (ii) VBIPV-E: A unit size vertical BIPV (i.e. 90° tilt) facing east and (iii) VBIPV-W: A unit size vertical BIPV (i.e. 90° tilt) facing west.

A multi-objective optimization approach is applied using a Genetic Algorithm (GA) to identify the most effective combinations of rooftop BIPV-PV and vertical BIPV configurations. The GA is selected due to its suitability for problems with non-linear, multi-modal objective functions and large solution spaces. It mimics natural selection by evolving a population of candidate solutions over successive generations, using operators such as selection, crossover, and mutation to explore the search space efficiently.

In this study, a GA is applied to optimize the azimuth angles of the two vertical BIPV systems, within the following bounds: VBIPV-E is constrained between 0° and 180°, while VBIPV-W is constrained between 180° and 360°. The full semi-circular range is used instead of pre-constraining BIPV orientations to fixed ranges (e.g., 75°–105° for east) to preserve generality and avoid introducing selection bias. The rooftop BIPV-PV remains fixed at the equator-facing orientation to ensure consistent comparison.

The GA optimization uses a population size of 150 and allows a maximum of 200 generations. The termination criteria are as follows: either (i) the geometric average of the relative change in Pareto front spread over the last 50 generations falls below 10^{-4} and the current spread is less than the mean spread during that period, or (ii) when the

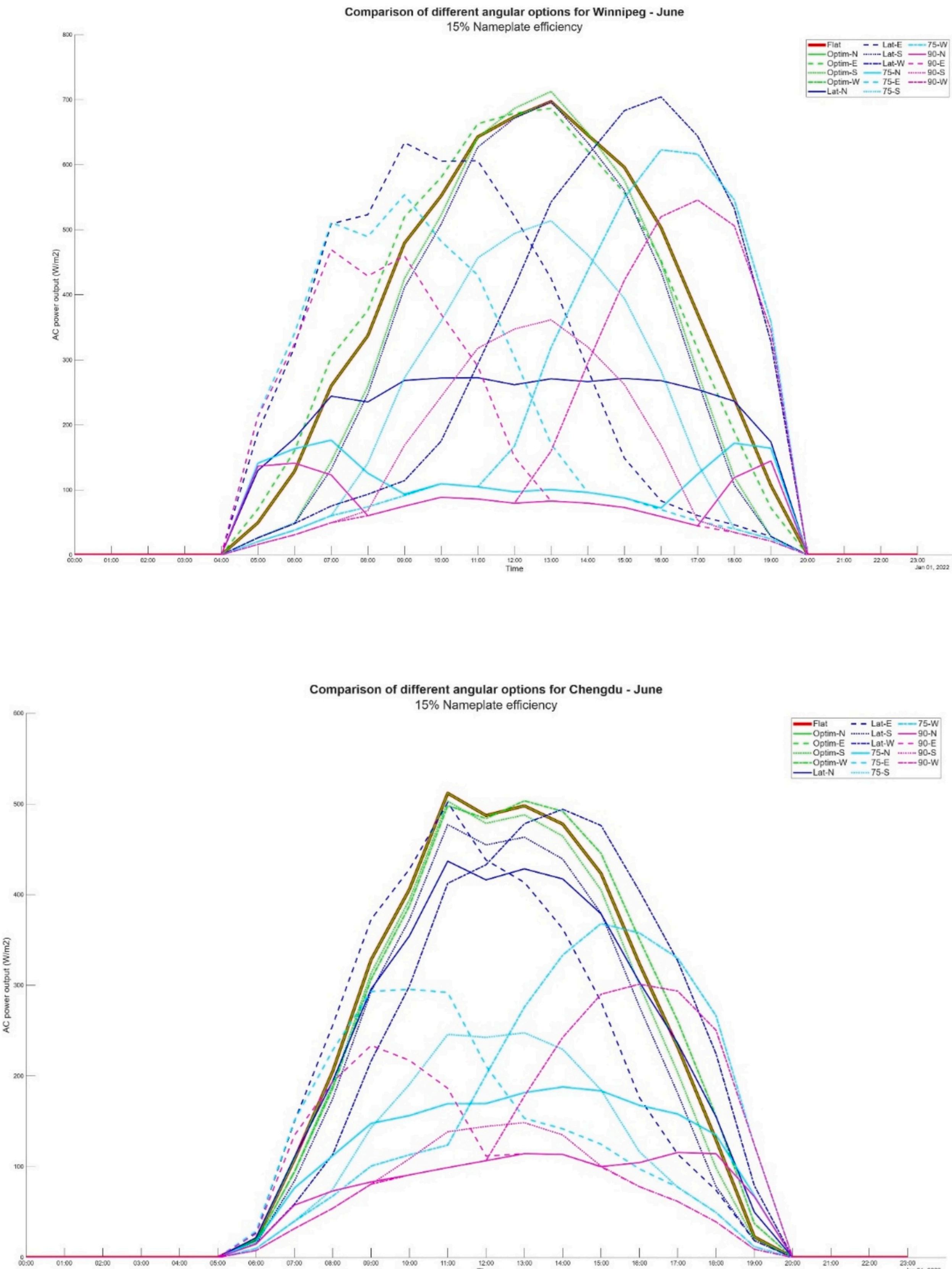

Fig. 3. An example of hourly average AC power output of BIPV modules for different angular configurations.

maximum number of 200 generations is reached. Across all 44 cities, the optimization met the first convergence criterion, indicating convergence to stable, well-defined solutions (see supplementary Note 2).

Three objective functions are formulated to guide GA optimization process.

2.2.3.1. Objective1: temporal complementarity and coupling. The alignment and offset between vertical BIPV and optimal-yield rooftop BIPV-PV generation profiles are assessed using a cross-correlation metric. This highlights how effectively vertical BIPV "fills in" when rooftop BIPV-PV underperforms (e.g., mornings, late afternoons, or during seasonal dips), favouring configurations where the two systems reduce volatility.

First, hourly generation pattern for the three systems is simulated and for each day cross-correlation coefficient and corresponding lag values are computed for east-facing vertical BIPV versus rooftop BIPV-PV, and west-facing BIPV systems versus rooftop BIPV-PV using valid generation hours (when at least one of the three systems has a generation value above 0). The lag associated with the maximum correlation coefficient is selected for each pair and a directional reward is assigned based on whether VBIPV-E leads and VBIPV-W lags relative to rooftop BIPV-PV. This approach ensures the following: Firstly, the VBIPV-E and VBIPV-W have a similar pattern with the rooftop BIPV-PV; Secondly, the vertical BIPV system patterns should be leading or lagging the rooftop BIPV-PV pattern. This approach tries to ensure combined output of three systems will provide longer coverage, and more evenly distributed generation peak across the day.

```
%% Cross-correlation signal coupling.
%% approach--------------------------------------.
[cc1, lags1] = xcorr(valid_bipv1, valid_baseline, 'coeff'); % East (bipv1) vs roof.
[~, idx1] = max(cc1);
bestLag1 = lags1(idx1); % If bestLag1 < 0 → bipv1 leads.
[cc2, lags2] = xcorr(valid_bipv2, valid_baseline, 'coeff'); % West (bipv2) vs roof.
[~, idx2] = max(cc2);
bestLag2 = lags2(idx2); % If bestLag2 > 0 → bipv2 lags.
reward1 = max(0, -bestLag1); % More reward if bipv1 leads.
reward2 = max(0, bestLag2); % More reward if bipv2 lags.
%% ----------------------------------------------------------------------.
supplementaryScore(d) = 0.5 * (reward1 + reward2);
```

A daily reward is then calculated for each day of the total simulation length (8760 h over 365 days), namely the 'supplementaryScore' as outlined in the code sample above, which is the average of the two rewards of leading and lagging effects provided by vertical BIPV. For the entire year, objective function 1 is defined by the daily average of the supplementaryScore.

2.2.3.2. Objective 2: smoothness of generation pattern. In addition to the temporal coupling effects provided by vertical BIPV, the second objective function is defined to ensure the overall smoothness of the aggregated generation pattern. This is quantified using normalized statistical dispersion (e.g., standard deviation) of the combined hourly output, expressed as the ratio of daily standard deviation to the mean generation.

```
smoothness(d) = daily_std / mean(Valid_day_power); % normalized std.
```

The objective function value is then obtained as the annual average of daily smoothness score.

2.2.3.3. Objective 3: maximize total generation. To prevent the risk of GA optimization prioritizing Objectives 1 and 2, a third objective is introduced to maximize total system generation. This objective is defined as the annual total electricity produced by the combined rooftop BIPV-PV and vertical BIPV systems. The optimization objectives are formulated to evaluate not only the total energy yield, but also the temporal characteristics of PV generation, which are critical for effective integration into building and urban energy systems. Rather than relying solely on conventional energy-based metrics, this study introduces two additional indicators that capture the interaction between rooftop PV and façade-integrated BIPV systems.

Objective function 1 quantifies temporal complementarity using a cross-correlation and lag-based approach. Cross-correlation of time-series data has been utilized in previous studies for coupling and matching multiple generation sources [32], and to maximize power point tracking of the PV systems [33]. This formulation evaluates whether BIPV generation occurs before or after the peak output of rooftop PV, thereby extending the overall generation window. East-facing BIPV systems are expected to generate earlier in the day, while west-facing systems contribute later to the afternoon. By rewarding leading and lagging behaviour relative to rooftop PV, this objective promotes configurations that reduce temporal concentration of generation and improve intra-day coverage. Although this metric does not directly model load matching or curtailment, it serves as a proxy for enhancing self-consumption potential and reducing peak export conditions. Objective function 2 assesses the smoothness of the aggregated generation profile using a normalized measure of statistical dispersion. This reflects the degree of fluctuation in combined PV output over time. A smoother generation profile indicates more stable power delivery, which is beneficial for reducing ramping requirements, improving compatibility with building demand profiles, and lowering dependence on energy storage or grid balancing mechanisms. Objective function 3 maximizes the total annual energy generation, ensuring that improvements in temporal distribution are not achieved at the expense of overall system productivity.

Although the GA formulation includes three objective functions, the final compromise solution was selected primarily based on the Euclidean distance to the ideal point for Objective 1 and Objective 2 because the purpose of this optimisation step is to identify azimuth configurations that improve the temporal quality of rooftop–façade PV coupling. Objective 3, total annual generation, is retained in the multi-objective optimisation to prevent the search from favouring low-yield solutions that may appear highly complementary or smooth only because generation is reduced. Therefore, Objective 3 acts as a yield-preservation criterion within the Pareto optimisation, while the final compromise selection prioritises the two generation-shaping objectives: temporal complementarity and smoothness. This selection strategy reflects the observed trade-off between generation shaping and yield maximisation: configurations that maximize total annual yield tend to concentrate generation around periods of high solar exposure, whereas configurations that improve complementarity and smoothness distribute generation more effectively across the day (See Appendix A).

The objective functions are selected to represent the core technical dimensions of rooftop–façade PV coupling rather than the full set of economic or policy-related performance indicators. Specifically, the optimisation aims to capture: (i) temporal complementarity between rooftop PV and BIPV generation profiles, (ii) smoothness of the aggregated generation pattern, and (iii) total annual generation. These objectives are chosen because they jointly describe when electricity is generated, how evenly the combined system generates electricity, and how much electricity is produced. Other economic indicators, such as payback period or electricity cost impacts, are evaluated separately in the techno-economic assessment and were therefore not included in this technical coupling optimisation.

2.2.3.4. Area ratio between vertical BIPV and optimal-yield rooftop BIPV-PV systems. To complement the temporal performance-based optimization, a follow-up analysis is conducted to evaluate the area efficiency of different BIPV configurations. While the GA focused on improving generation smoothness and temporal complementarity (Objectives1&2), it does not directly prioritize total energy output.

Therefore, this analysis investigates how much vertical BIPV area would be required to match the energy output of an optimal-yield rooftop BIPV-PV installation. East-facing and west-facing vertical BIPV configurations refer to azimuth angles obtained from the GA compromise solution, specifically Pareto-optimal points selected for their minimal distance to the ideal Objective1&2 values. These configurations are optimized to shape the temporal generation profile rather than maximize annual output. For benchmarking, an equator-facing vertical BIPV system and a conventional rooftop BIPV-PV system (with optimal tilt and equator-facing azimuth) are also modelled. All systems are assumed to have identical nameplate efficiencies, enabling a direct comparison of energy output per unit area.

2.3. Economic assessment

2.3.1. Economic data collection

The economic evaluation is based on a set of key variables that directly influence the economic performance of the BIPV systems. These include the country and city defining the geographical context of the analysis, discount rate (%), BIPV price (USD/m^2), conventional material replacement benefits (USD/m^2), electricity price (USD/kWh) and electricity price change rate (%/year). The complete dataset, including conventional material replacement benefits, electricity price, electricity growth rate and capital price change is tabulated in Appendix B.

BIPV price represents cost of installing BIPV per square meter for each application type. The prices of the selected BIPV applications are compiled from published databases and categorized into low, medium, and high price ranges for each integration typology. Table 4 presents the resulting cost ranges across all BIPV application types considered in this study. These price ranges are used to evaluate the sensitivity of economic performance to capital cost variations.

Conventional material replacement benefits reflect the avoided cost of conventional building materials replaced by BIPV module, incorporated as a cost offset in the economic analysis. This study considers eight BIPV applications that replace eight most popular conventional materials, suggested by local co-authors, in consultation with experienced professionals, or in accordance with country-specific guidelines [37–46]. The economic assessment considered only the direct material cost of the replaced conventional material (Appendix B). Additional costs such as installation and other soft costs are excluded as these add-on costs can vary significantly depending on system configuration and specific building contexts, which are beyond the scope of this study.

The electricity price is the reference electricity price of each city and electricity price change rate is the increase or decrease rate of the electricity price in each city, which captures the variation in electricity prices. The economic assessment is based on the most recent country-specific electricity prices and electricity growth rate. Electricity prices [47], electricity price change [48] are obtained from recent databases and published articles.

The discount rate is used to calculate the present value of life-cycle costs and benefits, directly influencing both effective LCOE and effective NPV. The discount rate is informed by the financial parameters and sensitivity of effective LCOE outcomes to weighted average cost of capital and other economic assumptions discussed in prior studies [49]. Based on multi-regional experience in the energy sector, the authors determined discount rates of 9.0% for developed countries and 12.5% for developing countries.

Table 4
Price ranges of each BIPV application.

Types	Lowest price (USD/m^2)	Medium price (USD/m^2)	Highest price (USD/m^2)	Sources
Continuous roof	$ 272.00	$ 741.50	$ 1211.00	[34–36]
Discontinuous roof	$ 227.00	$ 842.50	$ 1458.00	[34,35]
Skylight	$ 403.00	$ 630.50	$ 858.00	[34]
Rainscreen	$ 133.00	$ 811.50	$ 1490.00	[34–36]
Balcony balustrade	$ 133.70	$ 746.85	$ 1360.00	[34]
Shading device	$ 593.00	$ 1152.50	$ 1712.00	[34]
Double skin façade	$ 503.30	$ 503.30	$ 503.30	[34]
Curtain wall	$ 388.00	$ 763.50	$ 1139.00	[34,35]

2.3.2. Economic performance evaluation

Following the collection of economic input data, the economic performance of the BIPV systems is evaluated using effective NPV, effective discounted payback period, and effective LCOE. To capture the dual functionality of BIPV systems, these metrics explicitly incorporate both energy generation benefits and the benefits from conventional material replacement. The calculations follow the methodology proposed by [50] and are aligned with IEA-PVPS guidelines [51]. The core principle behind these metrics is that the cost of conventional materials is avoided due to their replacement by BIPV modules.

Effective NPV integrates lifecycle energy savings, grid export revenue, and cost offsets from conventional material replacement, discounted over the system life span. Effective NPV calculation is given by eq. (7) [48,49].

$$\textbf{\textit{Effective NPV}} = \boldsymbol{RB} - \boldsymbol{CC} + \boldsymbol{P_1} + \sum_{Year=2}^{LifeSpan} \frac{\boldsymbol{P_1} * (1 - \boldsymbol{DR})^{Y-1} - \boldsymbol{MC} + \boldsymbol{SV}_{Y=LifeSpan}}{(1 + \boldsymbol{R})^{Y-1}} \tag{7}$$

Where, ***RB*** is the replacement benefit of replacing conventional materials with BIPV ***CC***; is the total capital cost of BIPV product, inverter, and installation, assumed to be 120% of the BIPV system cost; $\boldsymbol{P_1}$ is the year 1 energy saving from electricity generation, calculated with total electricity generation (kWh) times electricity price (USD/kWh); ***LifeSpan*** is the total lifespan of the BIPV system, assumed to be 30 years within economic analysis of the performance indicators, and 25–50 years range within sensitivity analysis; ***DR*** is the degradation of PV generation over the year, assumed to be 0.5% per year; ***MC*** is the maintenance cost, assumed to be 1% of the CC; ***SV*** is the savage value calculated at the end of lifespan, assumed to be 5% of the CC; ***R*** is the discount rate for the lifecycle analysis.

The effective discounted payback period is calculated along with the NPV calculation (eq. (7)), where payback period is recorded at the year when cumulative discounted cashflow of eq. (7) reaches 0. Effective LCOE represents the net cost of electricity generation after accounting for conventional material replacement benefits and life cycle costs. Effective LCOE calculation is given by eq. (8),

$$\textbf{\textit{Effective LCOE}} = \frac{(\boldsymbol{CC} - \boldsymbol{RB}) + \sum_{Year=2}^{LifeSpan} \frac{\boldsymbol{MC} - \boldsymbol{SV}_{Y=LifeSpan}}{(1+\boldsymbol{R})^{Y-1}}}{\sum_{Year=1}^{LifeSpan} \boldsymbol{P_1} * (1 - \boldsymbol{DR})^{Y-1}} \tag{8}$$

2.3.3. Correlation analysis

Correlation analysis is conducted to identify how variations in key technical and financial parameters influence effective NPV across a wide range of plausible conditions. While the preceding economic assessment focused on specific cities, influential variables such as discount rates, conventional material replacement benefits, and electricity tariffs can vary substantially across regions, market cycles, or application contexts. Therefore, each parameter is defined by a minimum and maximum value derived from the aggregated city-level profile and economic data used in this study, to ensure realistic and representative sampling across multi-regional contexts. Table 5 summarises the parameter ranges used in the correlation analysis.

A 30-year system lifetime was adopted as the baseline assumption for the economic analysis. In the sensitivity analysis, system lifetime was treated as an uncertain parameter ranging from 25 to 50 years. The lower bound reflects a conventional PV project lifetime, while the upper

Table 5
Parameter boundaries of the correlation analysis and GSA.

Parameter	Lower Bound	Upper Bound	Units
Electricity Generation	10	500	$kWh/m^2/year$
BIPV Price	130	1800	USD/m^2
Discount Rate	0.05	0.13	–
Lifespan	25	50	years
Electricity Price	0.01	0.30	USD/kWh
Electricity Price Growth Rate	−10	20	%/year
Conventional Material Replacement Benefits	30	800	USD/m^2
BIPV/Conventional Material Price Ratio	Derived	Derived	Dimensionless

bound was included as an exploratory scenario to account for the building-integrated nature of BIPV, where PV elements may be considered together with longer building-envelope component lifecycles. The 50-year value was therefore not used as the baseline economic lifetime, but only as an upper-bound sensitivity case to evaluate the influence of extended service-life assumptions on economic performance.

Each sampled combination is input into the effective NPV evaluation model and resulting effective NPV values are recorded. Subsequently, Pearson's correlation coefficient is calculated between each input parameter and the resulting effective NPV array to establish an estimate of linear relationship between the two. The results are presented in Table 7.

2.3.4. Sensitivity analysis

To further investigate the influence of model inputs beyond linear relationships, global sensitivity analysis (GSA) is conducted using the variance-based Sobol method. GSA captures nonlinearities and input interdependencies across the full parameter space, making it suitable for nonlinear economic models with time-dependent financial structures. The model includes seven uncertain parameters: annual electricity generation, BIPV price, discount rate, system lifespan, electricity price, electricity price growth rate, and replacement benefit (modelled as the avoided cost of conventional materials). Each parameter is defined over a realistic range derived from market data and technical assumptions. In the absence of specific probability distributions, all parameters are assumed to follow uniform distributions bounded by their minimum and maximum values. Sobol analysis is implemented using the SALib Python library with Saltelli's sampling scheme to generate an input sample matrix, which ensures robust estimation of both first-order and second-order Sobol indices. A total of 50,000 base samples is generated, resulting in approximately 800,000 model evaluations when accounting for the extended matrix required for full second-order analysis. The effective NPV model is evaluated externally, and the outputs are used to calculate sensitivity indices. First-order indices (S1) quantify variance contributions of each parameter in isolation, total-order indices (ST) capture combined effects including interactions, and second-order indices (S2) quantify contributions from parameter pairs, identifying synergistic or conditional relationships not evident from marginal effect. Sensitivity results are visualized using bar plots and interaction heat maps to highlight dominant parameters and key interactions.

3. Results and discussion

3.1. BIPV energy-related assessment

The annual electricity output of the selected BIPV applications is simulated across 17 angular configurations (see Table 2), in combination with nameplate module efficiencies. At the lowest efficiency (5%), annual yields ranged from less than 25 to more than 50 kWh/m^2, while at higher efficiencies (25%), outputs spanned 120–260 kWh/m^2. The optimal tilt angles for each city for maximum annual electricity generation under each cardinal azimuths and the best and second-best orientation and tilt combinations for rooftop and façade BIPV across all cities are summarized in Supplementary Material S1.

For rooftop BIPV-PV, conventional design often aligns panel tilt with local latitude, labelled above as "latitude orientation". However, our studies confirm consistent deviations from this rule (see Supplementary Table 1). For example, Australian cities such as Melbourne (∼37.8°S), Rockhampton (∼23.4°S), and Wagga Wagga (∼35.1°S) exhibited optimal tilt angles lower than their latitudes. Similarly, high-latitude cities like Yellowknife, Canada (62°27′N), and Kiruna, Sweden (67°50′N), showed optimal tilts (57.76° and 52.46°, respectively). These deviations are largely attributable to solar position, climate factors, atmospheric light-scattering, and the seasonal solar irradiance balance. Locations with frequent cloud cover or substantial diffuse radiation benefit from smaller tilt angles, allowing the modules to capture diffuse sunlight more effectively due to a higher view factor of the sky. Additionally, smaller angles enhance summer generation, which can dominate annual yield in regions with clearer summer conditions.

Most cities achieved peak performance with an optimal tilt angle paired with an equator-facing orientation; north-facing in the southern hemisphere and south-facing in the northern hemisphere, consistent with conventional PV design principles (see Supplementary Table 2). Exceptions are found in equatorial cities such as Jakarta, Medan, Singapore, and Teresina, where east- or west-facing orientations outperformed equator-facing panels due to the high solar altitude path yielding more symmetrical irradiance throughout the day and reducing the dominance of equator-facing configurations.

For façade BIPV, all top-performing configurations employed a 75° tilt to enhance irradiance capture near solar noon, when the sun was highest in the sky. In many cities, particularly those above 35° latitude; the second-best options featured a 90° vertical tilt, indicating that vertical façades remain capable of substantial annual generation, especially in mid-latitude to high-latitude regions with persistently low solar elevation. Many high-performing façade configurations had east or west-facing azimuths, indicating that non-equator-facing façades can generate valuable electricity during morning and late afternoon hours, supporting load-matching and offering greater architectural flexibility without significant energy loss.

When the average hourly output is considered (see example in Fig. 2), BIPV systems with different angular configurations exhibited distinct power generation patterns, diverging especially between rooftop and façade BIPV designs. This highlights the potential for synergistic BIPV combinations to enhance energy resilience. However, realizing this potential requires more detailed data analysis and rigorous evaluation procedures.

To further explore the practical potential of synergistic BIPV combinations, vertical BIPV (i.e., 90° tilt) is selected for detailed assessment. This configuration is less sensitive to dirt accumulation and poses fewer spatial challenges compared to rooftop BIPV-PV installations, making it a realistic and scalable option for widespread urban deployment. It is also more common and compatible with standard façade designs than systems installed at a 75° tilt.

To evaluate its performance, annual average daily generation profiles of optimally tilted, equator-facing rooftop BIPV-PV and vertical BIPV systems are compared. Rooftop BIPV-PV and vertical BIPVs are assigned 20% efficiency to unify the product specification) (see Appendix C). Rooftop BIPV-PV delivered higher yields in most cities due to their greater efficiency and optimal tilt/azimuth alignment. However, vertical BIPV exhibited clear diurnal and seasonal complementarity in higher-latitude cities. Such complementarity indicates that integrating rooftop BIPV-PV and vertical PV systems can smooth daily and annual generation profiles, reduce seasonal variability and enhance overall energy availability. This flexibility is particularly beneficial for the building sector to maximize energy ownership and suggests an integrated design approach leveraging their complementary temporal generation can enhance overall system performance. Thereby, the detailed synergy between rooftop BIPV-PV and vertical BIPV systems is further investigated next.

3.2. Coupling of vertical BIPV and optimal-yield rooftop BIPV-PV

Multi-objective optimizations, using genetic algorithm (GA) targeted three objectives: (1) temporal complementarity, (2) generation smoothness, and (3) total electricity output. Existing studies [52] focuses on energy outputs (i.e. Objective 3); however, overlooked the flexibility contributions of vertical BIPV as explained in the last section [53–55]. This study advances this approach by balancing all three objectives simultaneously. The results of the multi-objective optimization, trade-offs among temporal complementarity, generation smoothness, and total annual yield are presented in Supplementary Material S2.

Optimization solutions are selected from the Pareto front (Supplementary Fig. 1) by minimizing the Euclidean distance to the ideal point for Objectives 1 and 2, identifying optimal azimuth angle pairs for east- and west-facing vertical BIPV across multiple cities. The average hourly generation profile (see Appendix D) demonstrates how azimuth design choices translate into real-world power distribution across the day. Rooftop BIPV-PV peaks at noon, while VBIPV-E and VBIPV-W dominate in the morning and afternoon, respectively. Their combined output produces a flatter, more stable profile with reduced ramp rates. The azimuth angles obtained from this optimization (Pareto-optimal points; selected based on their minimal Euclidean distance to the ideal values of Objectives 1 and 2) are then used for subsequent analysis.

To complement the temporal performance analysis, the area ratio (i.e. ratio of annual rooftop BIPV-PV yield to the annual yield of east-facing and/or west-facing vertical BIPV) is evaluated by comparing the vertical BIPV area required to match the annual output of an optimally tilted, equator-facing rooftop BIPV-PV with the same system efficiency (see Materials and methods; 2.2.3). Table 6 summarises the required vertical BIPV area relative to rooftop BIPV-PV to achieve equivalent annual electricity generation.

As tabulated in Table 6, the selected cities average required vertical BIPV area is only 2, 2.5, and 1.7 times that of rooftop BIPV-PV for east-only, west-only, and equator-only orientations, respectively. When combined orientations are considered, the selected cities average required vertical BIPV area to match rooftop BIPV-PV output is twice for an equally distributed east–west–equator combination and 2.2 times larger for an equally distributed east–west combination.

As efficiency scales linearly in our performance model, the ratio can be adjusted by multiplying by the efficiency factor; for instance, if the rooftop BIPV-PV operates at 1.5 times the efficiency of the vertical BIPV, the required vertical BIPV area should be increased by the same factor. Therefore, even if vertical BIPV is only half as efficient as rooftop BIPV-

Table 6
Vertical BIPV area ratio to the rooftop BIPV-PV area that reaches equal generation.

Country	City	East Only	West Only	Equator Only	East + West + Equator distributed equally	East + West distributed equally
China	Chengdu	2.2	1.9	1.7	1.9	2.0
China	Beijing	2.2	2.6	1.4	1.9	2.4
China	Xining	2.4	2.1	1.4	1.9	2.3
China	Shenyang	1.8	2.9	1.3	1.8	2.3
China	Guangzhou	2.0	2.1	1.7	1.9	2.1
China	Shanghai	1.5	2.6	1.7	1.8	1.9
Japan	Aomori	1.5	2.4	1.6	1.8	1.8
Japan	Tokyo	1.8	2.8	1.5	1.9	2.2
Japan	Fukuoka	2.1	2.4	1.7	2.0	2.3
South Korea	Seoul	2.2	2.6	1.5	2.0	2.4
South Korea	Daejeon	2.1	2.5	1.5	2.0	2.3
South Korea	Gwangju	2.2	2.6	1.6	2.0	2.4
South Korea	Busan	2.2	2.6	1.5	2.0	2.4
Singapore	Singapore	1.9	1.7	2.4	2.0	1.8
Indonesia	Jakarta	1.3	2.3	1.8	1.7	1.6
Indonesia	Medan	1.7	1.9	2.1	1.9	1.8
Nigeria	Port Harcourt	1.9	2.1	2.2	2.1	2.0
Nigeria	Abuja	1.9	2.2	2.2	2.1	2.0
Nigeria	Kaduna	1.9	2.1	2.2	2.1	2.0
Nigeria	Kano	1.9	2.1	2.2	2.1	2.0
Canada	Toronto	2.1	2.6	1.5	2.0	2.3
Canada	St. Johns	1.8	2.4	1.4	1.8	2.0
Canada	Winnipeg	2.5	2.5	1.4	1.9	2.5
Canada	Yellowknife	2.1	2.6	1.2	1.8	2.3
USA	Portland	2.2	2.4	1.5	2.0	2.3
USA	Denver	1.8	3.3	1.4	1.9	2.3
USA	Atlanta	2.1	2.6	1.6	2.0	2.4
USA	Albuquerque	2.3	3.3	1.6	2.2	2.7
USA	Phoenix	2.4	3.0	1.7	2.2	2.7
Brazil	Curitiba	2.2	2.4	1.8	2.1	2.3
Brazil	Rio	1.7	2.8	1.8	2.0	2.1
Brazil	Cuiaba	1.6	3.0	1.8	2.0	2.1
Brazil	Teresina	1.3	2.8	2.3	1.9	1.8
Spain	Gijon	2.3	2.1	1.5	1.9	2.2
Spain	Madrid	2.6	2.5	1.6	2.1	2.5
Spain	Malaga	2.7	2.3	1.6	2.1	2.4
Sweden	Stockholm	1.9	2.3	1.3	1.7	2.1
Sweden	Lund	2.1	2.2	1.4	1.8	2.2
Sweden	Kiruna	2.0	2.2	1.3	1.7	2.1
Australia	Melbourne	2.0	2.5	1.6	2.0	2.2
Australia	Rockhampton	1.4	2.5	1.8	1.8	1.8
Australia	Wagga Wagga	2.2	2.7	1.6	2.1	2.4
Australia	Adelaide	1.7	2.9	1.5	1.9	2.1
Australia	Broome	1.7	3.0	1.9	2.1	2.2
	Average	2.0	2.5	1.7	2.0	2.2

PV due to shading or tilt, the additional area needed to generate the same amount of electricity is still within the reasonable building surface, demonstrating that vertical BIPV is still a viable option. However, this interpretation does not account for practical building constraints such as window-to-wall ratio, shading and obstruction, fire safety regulations, maintenance access, daylighting requirements, and architectural design limitations; therefore, detailed building-level simulations would be required for implementation assessment. This is especially relevant for medium- to high-rise buildings, where rooftop space is limited or occupied. Moreover, optimizing temporal complementarity and smoothness does not substantially increase the required area, supporting the viability of vertical BIPV.

3.3. BIPV economic assessment

Historically, economic performance of renewable energy technologies has been evaluated by using Net Present Value (NPV) and Levelized Cost of Electricity (LCOE) [56,57]. Due to conventional calculation methods failing to account for the dual functionality of BIPV, the economic potential of BIPV is often undervalued. To address this, this study adopts effective NPV, effective LCOE, and effective discounted payback period as defined in IEA-PVPS guidelines [58,59] (see Materials and methods; 2.3.2). The analysis includes only conventional material cost offset, excluding add-on costs (e.g. additional installation and soft costs associated with BIPV compared to conventional materials). This is because the add-on installation and soft costs [60] vary significantly across building contexts. When interpreting the results, it should be noted that the BIPV prices (see Table 4), include combined module and add-on installation and soft costs; hence, the reported values should be interpreted as indicative rather than absolute. Further, the assessment considers the aforementioned efficiency range to identify the minimum efficiency required to achieve economic viability under each BIPV price scenario as well as the average payback years across efficiency range within different BIPV price bands (See Appendix E).

At low BIPV prices (133–600 USD/m^2 depending on application, Table 4), more than 90% of configurations became economically viable (effective NPV $\geq$ 0; effective LCOE $\leq$ reference electricity price) starting from efficiencies of around 18%, and in some cases even lower. As BIPV price increases to medium (500–1160 USD/m^2 depending on the applications) and high levels (500–1720 USD/m^2 depending on the applications), viability remained substantial, as more than half of the configurations according to effective NPV and nearly 80% of configurations according to effective LCOE achieved viability with 18% or higher efficiency, and even lower values in some cases. These results demonstrate the competitiveness of BIPV systems even under elevated price scenarios, contrasting with prevailing perception of BIPV as a high-cost technology, especially in the future if additional installation and soft costs can be minimized through training and knowledge sharing.

Across applications, double-skin façades (DSF) and skylights consistently demonstrated favourable performance in most cities under both effective LCOE and effective NPV viability criteria, as well as achieved acceptable payback period across the price bands, due to their high conventional material replacement benefits. In contrast, shading devices consistently showed limited viability: under effective NPV, nearly half of the cities faced challenges in achieving economic viability at a medium BIPV price, while under effective LCOE, one-fourth of cities required 19–25% efficiency to achieve viability at the same price. This is mainly due to the low conventional material replacement benefits. Similarly, the average payback period steeped towards over 30 years within the high BIPV price band for many of the cities. In general, when the cost of conventional material replacement is high, BIPV applications are more likely to achieve economic competitiveness.

Across the countries, Australia, Singapore, South Korea, and Japan demonstrated favourable economic performance, with all BIPV applications achieving positive effective NPVs and reasonable payback year even for the high BIPV price category for a minimum efficiency of 18%, or occasionally still lower (Appendix F). In these countries, grid parity; where the cost of BIPV electricity equals grid prices is also reached under high BIPV price conditions at similar efficiency levels. This is primarily attributed to high electricity prices, high electricity price growth, and substantial conventional material replacement benefits in these regions. In addition, according to the effective LCOE metric, Brazil and Spain achieve grid parity across all applications for the high BIPV price category at minimum efficiency of 18% or lower in some cases. According to the effective NPV metric, for the medium BIPV price category, all the applications in Spain and China demonstrated viability at an 18% efficiency threshold or lower in some cases. These trends reflect the influence of high electricity price (Spain) and electricity price growth (China) (see Appendix B).

According to the International Renewable Energy Agency (IRENA) [61], the global average LCOE for utility-scale solar PV reached USD 43/MWh in 2024. The corresponding average effective LCOE values of the selected BIPV applications, across nameplate efficiencies and price categories, are compared with the values above and are displayed in Fig. 4.

As shown in Fig. 4, when BIPV prices are high, the average effective LCOE values exceed those of utility-scale PV. However, at medium BIPV prices, effective LCOE values become comparable to or lower than utility-scale PV when the efficiency reaches around 21% or higher. When BIPV prices are low, effective LCOE values fall below those of utility-scale PV for all studied efficiencies. As electricity prices are expected to rise in the future [62], the effective LCOE values for BIPV could thus potentially decrease further.

It is important to note that the purpose of this analysis is not to prioritize specific locations for BIPV applications but to illustrate how economic performance varies based on local sensitivities to key input variables across different contexts. Overall, both effective NPV and effective LCOE outcomes are influenced by key input parameters, including electricity price, electricity price growth rate, BIPV price, and conventional material replacement benefits. A comprehensive correlation and sensitivity analysis is conducted to evaluate the relative impact of these variables, as detailed in the following section.

3.4. The Most influential parameters of economic performance

Correlation analysis is conducted to assess the directional influence of individual input parameters. While this study considers an operational lifespan range from 25 to 50 years, BIPV may continue to generate electricity up to this period [63]. To examine this effect, the performance across multiple lifespan scenarios is assessed. The results of this analysis are tabulated in Table 7, which summarises the correlation between key input variables and both economic indicators under different lifespan assumptions.

Electricity price growth exhibits the strongest positive correlation with effective NPV. Electricity generation, electricity price and conventional material replacement benefits also correlate positively, though their influence declines with increasing lifespan. BIPV prices consistently correlate negatively with effective NPV. However, this negative effect weakens over longer lifespans, indicating that extended generation can offset initial investment. The discount rate shows a moderate negative correlation, highlighting its impact on long-term returns.

By contrast, effective LCOE correlations differ; electricity generation has the strongest negative correlation (i.e. more generation means lower effective LCOE), while the BIPV price correlate positively, directly contributing to price burden. The discount rate and electricity-related parameters show minimal influence on the effective LCOE, whereas conventional material replacement benefits exhibit a moderate negative correlation, particularly over shorter lifespans, suggesting that material offsets marginally improve cost competitiveness. Lifespan extensions have a negligible effect on effective LCOE correlations compared to their significant impact on effective NPV.

To capture the combined and nonlinear influence of these

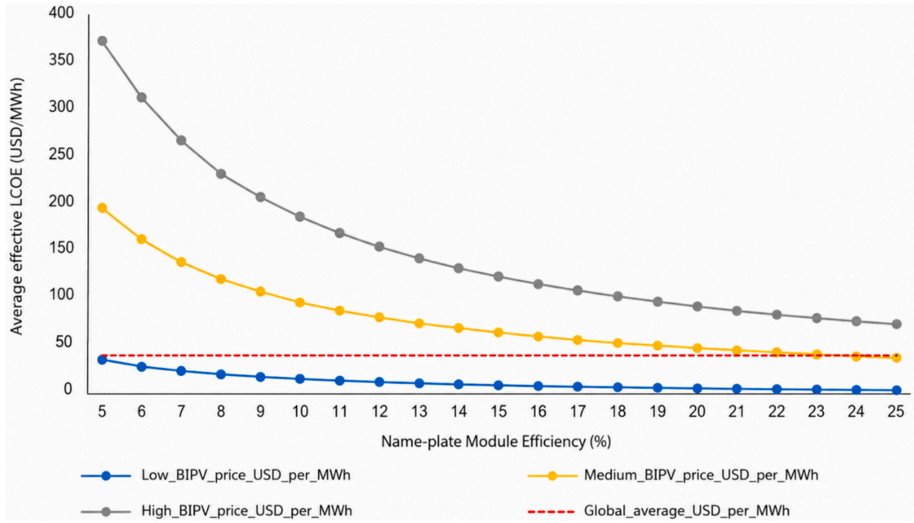

Fig. 4. Average effective LCOE values of BIPV across nameplate efficiencies. Average effective LCOE values (USD/MWh) are shown (USD/MWh) for low (133–600 USD/m^2), medium (500–1160 USD/m^2), and high (500–1720 USD/m^2) BIPV prices versus efficiency levels from 5% to 25%.

Table 7
Results of correlation analysis.

Parameter	Correlation with 'Life Span' for effective NPV		
	25 years	25–30 years	50 years
'Electricity Generation'	0.3394	0.3129	0.1680
'BIPV Price'	−0.3410	−0.2762	−0.0290
'Discount Rates'	−0.1651	−0.1633	−0.2013
'Life Span'	NaN	0.0539	NaN
'Electricity Price'	0.3279	0.3161	0.1672
'Electricity Growth'	0.4843	0.4853	0.3960
'Conventional Material Replacement Benefits	0.1349	0.1038	0.0169
'BIPV/Conventional Material Price Ratio'	−0.1999	−0.1622	−0.0256
	Correlation with 'Life Span' for effective LCOE		
Parameter	25 years	25–30 years	50 years
'Electricity Generation'	−0.4104	−0.4123	−0.4097
'BIPV Price'	0.3933	0.3884	0.3901
'Discount Rates'	0.0139	0.0131	0.0212
'Life Span'	NaN	−0.0187	NaN
'Electricity Price'	−0.0028	0.0057	0.0054
'Electricity Growth'	0.0048	0.0062	0.0058
'Conventional Material Replacement Benefits	−0.1792	−0.1858	−0.189
'BIPV/Conventional Material Price Ratio'	0.2488	0.2466	0.2492

parameters, global sensitivity analysis (GSA) is performed using the variance-based Sobol method. The Sobol method decomposes the variance of model outputs into contributions attributable to individual input variables and their interactions. In this study, first-order Sobol indices are used to quantify the direct contribution of each input parameter to the variance of the economic performance metrics, while total-order indices capture both the direct effect of each parameter and its interaction effects with other parameters. Fig. 5 presents the Sobol-based sensitivity analysis results for effective NPV and effective LCOE across all input parameters. A higher Sobol index indicates that the corresponding input parameter has a stronger influence on the variability of the economic outcome under the tested parameter ranges.

For effective NPV (Fig. 5a), the first-order indices for all examined variables (electricity generation, discount rate, electricity price and BIPV price) are near zero, indicating minimal isolated impact on variance. In contrast, total-order indices are consistently high, indicating that effective NPV variance is primarily driven by parameter interactions. A similar trend is observed for effective LCOE (Fig. 5b).

Building on these findings, the second-order Sobol indices are further examined to explicitly quantify pairwise parameter interactions. Fig. 6 presents these second-order Sobol indices for both effective NPV and LCOE.

Detailed examination of second-order interactions (Fig. 6a), highlights dominant pairs influencing effective NPV variance: (conventional material replacement benefits × life span), (electricity generation × discount rate), (electricity price growth × discount rate) and (BIPV price × electricity generation). These interactions carry clear economic implications. For instance, the benefit of conventional material replacement is strongly influenced by the system lifespan, while the impact of electricity generation on effective NPV diminishes if future returns are heavily discounted. For effective LCOE (Fig. 6b), key interactions include (electricity price × BIPV price), (electricity generation × conventional material replacement benefits), (electricity price growth × BIPV price) and (conventional material replacement benefits × life span).

Overall, BIPV economic performance is governed by nonlinear, interdependent parameter interactions. Variables with negligible individual effects can become critical through these interactions, particularly in long-term financial contexts. This underscores that isolated interventions (e.g. product cost reductions) may be insufficient without integrated financial and market assessment. Future R&D should prioritize these key parameters to effectively enhance BIPV economic viability.

4. Conclusions

As a building-integrated solution, façade BIPV supports complementary and efficient electricity generation in urban environments. When combined with rooftop BIPV-PV, it provides temporal complementarity, smoother generation profiles, and improved seasonal balance. Strategic deployment of vertical BIPV with varied orientations can further enhance generation stability without substantially reducing overall energy yield in dense urban contexts. The findings of this study suggest that potential of BIPV may be more promising than is often assumed, both in terms of energy performance and economic feasibility.

The economic performance of BIPV is influenced by a combination of interrelated technical, financial, and market factors, suggesting that cost reduction alone may not be sufficient to achieve large-scale adoption. To accelerate BIPV adoption, technical improvements in efficiency and lifespan must go hand in hand with targeted training and knowledge-sharing initiatives that build industry capability and reduce soft costs

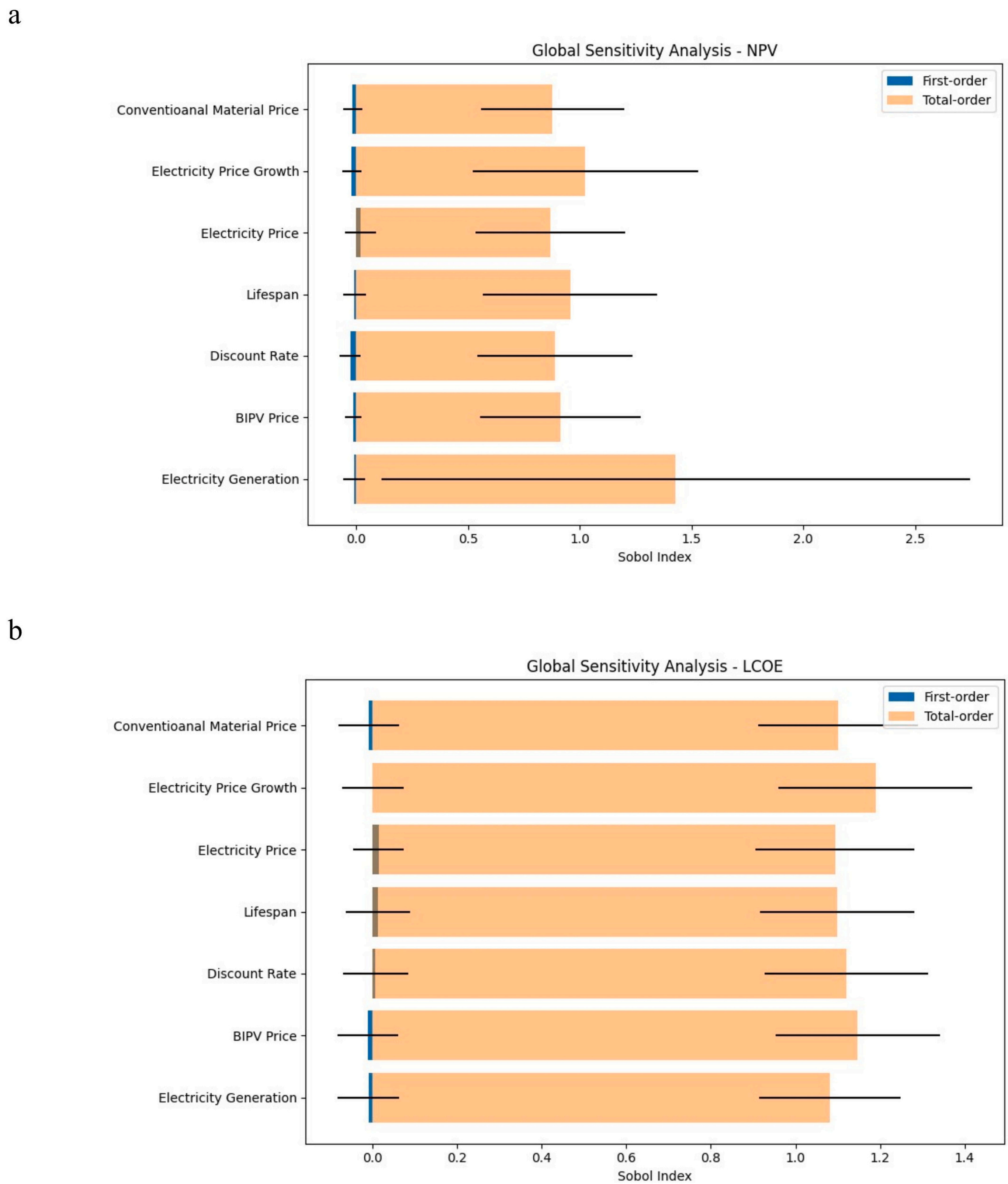

Fig. 5. Global sensitivity analysis of key economic metrics using Sobol indices. a, First-order and total-order Sobol indices for effective NPV. b, First-order and total-order Sobol indices for effective LCOE.

across design, construction, installation, and long-term operation. As the study aims to provide a generalised, screening-level assessment to support early investment decision-making, it does not incorporate detailed urban morphologies (e.g., building density, ambient and ground-reflected radiation, and shading). Given the complexity of BIPV system design, continued efforts in digitalization and system optimization, including those underway within IEA-PVPS Task 15, will be important to advance future integration and adoption.

This study also highlights the need for more coordinated and up-to-date data collection efforts at a multi-regional scale. Future research

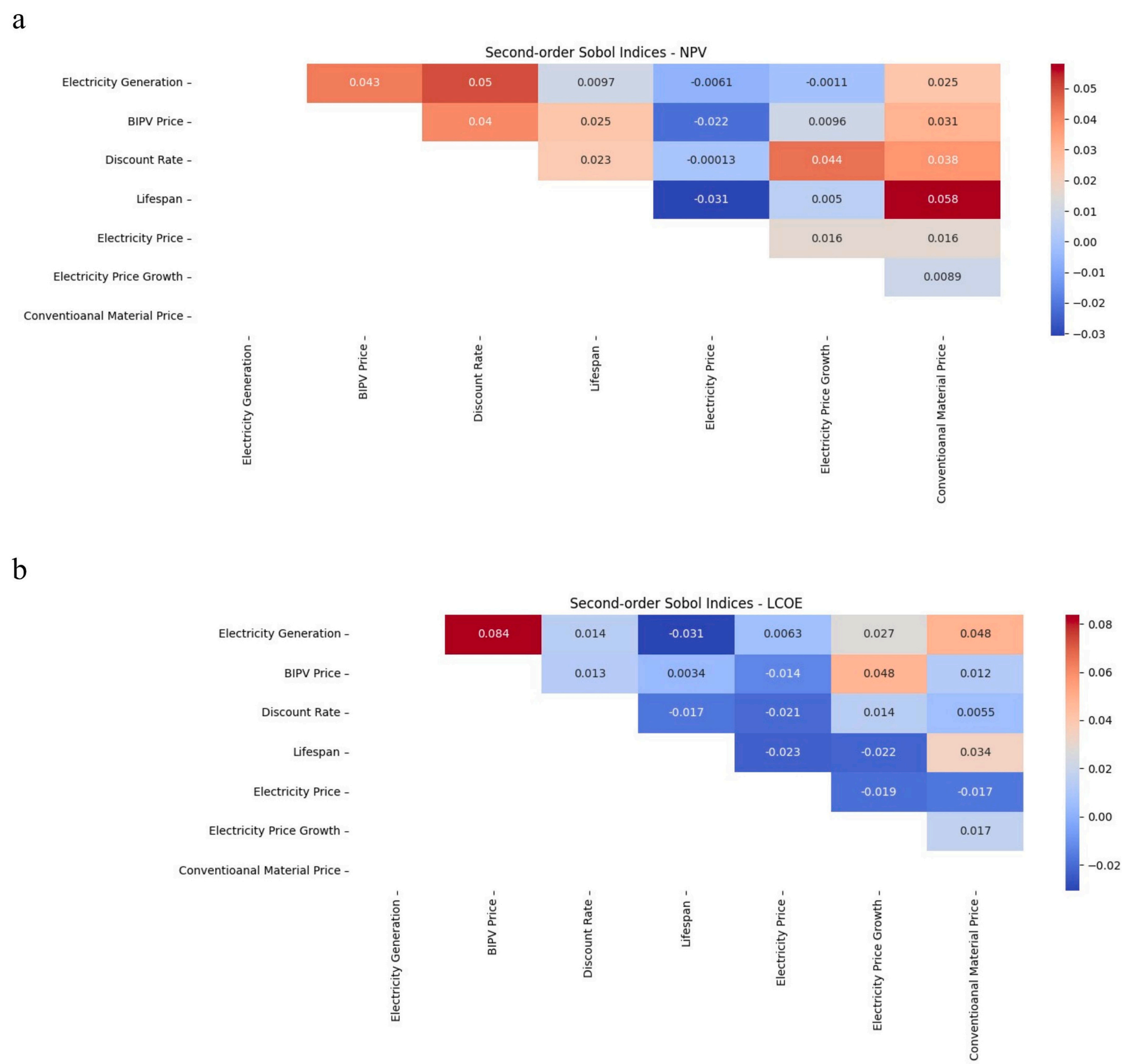

Fig. 6. Second-order Sobol indices showing interaction effects between paired variables. a, Interaction effects on effective NPV. b, Interaction effects on effective LCOE.

would benefit from strengthened international collaboration among academia, industry, and policymakers to develop and maintain comprehensive datasets of BIPV-related economic factors (such as maintenance cost, labour cost, inverter cost, etc.). Establishing such shared and regularly updated data repositories would significantly improve the accuracy, comparability, and practical relevance of techno-economic assessments, ultimately support more informed decision-making and accelerate the deployment of BIPV systems.

A key limitation of this study lies in the use of uniform system-level assumptions, including inverter efficiency, DC/AC ratio, albedo, temperature coefficient, and aggregate loss factors, across all BIPV applications and locations. This approach is adopted to ensure methodological consistency and enable comparative analysis across 44 cities and eight application types. However, it does not explicitly capture application-specific operational differences, including ventilation conditions, rear-side or backsheet temperature, shading and self-shading behaviour, soiling effects, optical properties, installation methods, mounting constraints, and local boundary conditions. These factors may vary substantially between roofs, curtain walls, rainscreens, double-skin façades, skylights, balustrades, and shading devices, and can influence both module operating temperature and effective irradiance. As a result, some performance variations between different BIPV configurations may be underrepresented. Therefore, the results should be interpreted as comparative scenario-based estimates under harmonised assumptions, rather than project-specific predictions for individual BIPV installations.

Future research should incorporate application-sensitive parameterisation and develop more refined modelling frameworks that account for thermal, optical, environmental, and installation-specific effects. In particular, integrating empirical datasets and conducting uncertainty or sensitivity analyses tailored to different BIPV applications would improve the robustness and practical relevance of large-scale techno-economic assessments.

CRediT authorship contribution statement

Rebecca Jing Yang: Writing – review & editing, Supervision, Project administration, Methodology. **Chengyang Liu:** Writing – original draft, Methodology, Formal analysis, Data curation. **Mathanky Sachchithananthan:** Writing – original draft, Data curation. **Nilmini Weerasinghe:** Methodology, Formal analysis. **Yukun Zang:** Methodology, Formal analysis. **Helen Rose Wilson:** Methodology, Formal analysis. **Jonathan Leloux:** Methodology, Formal analysis. **Daniel Valencia-Caballero:** Methodology, Formal analysis. **Clarissa Debiazi Zomer:** Methodology, Formal analysis. **Malin Unger:** Methodology, Formal analysis. **Francesco Frontini:** Methodology, Formal analysis. **Hisashi Ishii:** Methodology, Formal analysis. **Sajani Jayasuriya:** Methodology, Formal analysis. **Hongying Zhao:** Methodology, Formal analysis. **Shin Woei Leow:** Methodology, Formal analysis. **Rui Liu:** Methodology, Formal analysis. **Jose M. Vega de Seoane:** Methodology, Formal analysis. **Jun-Tae Kim:** Methodology, Formal analysis. **Philippe Macé:** Methodology, Formal analysis. **Chinemelu J. Anumba:** Methodology, Formal analysis. **Yusen Zhao:** Methodology, Formal analysis. **Michael Taylor:** Methodology.

Declaration of competing interest

The authors declare that they have no known competing financial interests or personal relationships that could have appeared to influence the work reported in this paper.

Acknowledgements

The authors thank Michael Woodhouse for his valuable contribution to the economic analysis presented in this study. The authors also acknowledge the support and contributions of the International Energy Agency Photovoltaic Power Systems Programme (IEA PVPS), Task 15.

Appendix A. Supplementary data

Supplementary data to this article can be found online at https://doi.org/10.1016/j.enbuild.2026.118031.

Data availability

All data supporting the findings of this study are included within the main manuscript and its supplementary materials

References

[1] IEA T15, International definitions of "BIPV.", Natural Resources Canada, 2018. https://iea-pvps.org/key-topics/international-definitions-of-bipv/.
[2] F.J.M.M. Nijsse, J.-F. Mercure, N. Ameli, F. Larosa, S. Kothari, J. Rickman, et al., The momentum of the solar energy transition, Nat. Commun. 14 (2023) 6542, https://doi.org/10.1038/s41467-023-41971-7.
[3] B. Svetozarevic, M. Begle, P. Jayathissa, S. Caranovic, R.F. Shepherd, Z. Nagy, et al., Dynamic photovoltaic building envelopes for adaptive energy and comfort management, Nat. Energy 4 (2019) 671–682, https://doi.org/10.1038/s41560-019-0424-0.
[4] A. Faes, A. Virtuani, H. Quest, L. Maturi, A. Scognamiglio, F. Frontini, et al., Building-integrated photovoltaics, Nat. Rev. Clean Technol. 1 (2025) 333–350, https://doi.org/10.1038/s44359-025-00059-9.
[5] J. Kong, Y. Dong, A. Poshnath, B. Rismanchi, P.S. Yap, Application of Building Integrated Photovoltaic (BIPV) in net-zero energy buildings (NZEBs), Energies 16 (2023) 6401, https://doi.org/10.3390/EN16176401.
[6] N. Skandalos, M. Wang, V. Kapsalis, D. D'Agostino, D. Parker, S.S. Bhuvad, et al., Building PV integration according to regional climate conditions: BIPV regional adaptability extending Köppen-Geiger climate classification against urban and climate-related temperature increases, Renew. Sust. Energ. Rev. 169 (2022) 112950, https://doi.org/10.1016/J.RSER.2022.112950.
[7] F. Meinardi, F. Bruni, S. Brovelli, Luminescent solar concentrators for building-integrated photovoltaics, Nat. Rev. Mater. 2 (2017) 17072, https://doi.org/10.1038/natrevmats.2017.72.
[8] P. Bonomo, F. Frontini, R. Loonen, A.H.M.E. Reinders, Comprehensive review and state of play in the use of photovoltaics in buildings, Energ. Buildings 323 (2024) 114737, https://doi.org/10.1016/J.ENBUILD.2024.114737.
[9] X. Qiao, T. Zhao, X. Zhang, Y. Li, Multi-objective optimization of building integrated photovoltaic windows in office building, Energ. Buildings 318 (2024) 114459, https://doi.org/10.1016/J.ENBUILD.2024.114459.
[10] J. Prakash, V. Shree, Economic viability of building-integrated photovoltaics (BIPV) in composite-climate public buildings: evidence from Hamirpur, India, Energy Sustain. Dev. 94 (2026) 102073, https://doi.org/10.1016/j.esd.2026.102073.
[11] M. Fariz, M. Sadeq, N. Sellami, Integrated simulation and optimisation framework for techno-economic evaluation of BIPV systems: a Scottish case study, E-Prime - Advances in Electrical Engineering, Electronics and Energy 13 (2025) 101091, https://doi.org/10.1016/j.prime.2025.101091.
[12] Y. Kang, Y. Cui, D. Zhang, W. Xu, F. Pang, S. Lu, et al., Comprehensive photovoltaic system in roofs, opaque walls, and windows toward zero-energy buildings utilizing multi-objective optimization, J. Build. Eng. 104 (2025) 112320, https://doi.org/10.1016/j.jobe.2025.112320.
[13] S.A. Restrepo, J. Morcillo, M. Castaneda, S. Zapata, A.J. Aristizábal, Experimental research on the performance of a BIPV system operating in Girardot, Colombia, Energy Rep. 9 (2023) 194–204, https://doi.org/10.1016/j.egyr.2023.05.256.
[14] M. Bagholizadeh, A.A. Nadooshan, S.A.H.H. Dehkordi, M. Rostamzadeh-Renani, R. Rostamzadeh-Renani, M. Afrand, Multi-objective optimization of annual electricity consumption and annual electricity production of a residential building using photovoltaic shadings, Int. J. Energy Res. 46 (2022) 21172–21216, https://doi.org/10.1002/er.8401.
[15] S. Miraba, A. Salehi, M. Rostamzadeh-Renani, R. Ehteshami, A. Shahbazi, R. Rostamzadeh-Renani, et al., Adaptive BIPV shading optimization for electricity generation and building electricity management, sDA, and DGP using multi-objective algorithms, Appl. Energy 402 (2025), https://doi.org/10.1016/j.apenergy.2025.126860.
[16] M. Bagholizadeh, S.A.H.H. Dehkordi, M. Rostamzadeh-Renani, R. Rostamzadeh-Renani, N.K. Azarkhavarani, D. Toghraie, Optimization of annual electricity consumption costs and the costs of insulation and phase change materials in the residential building using artificial neural network and genetic algorithm methods, J. Energy Storage 62 (2023) 106916, https://doi.org/10.1016/j.est.2023.106916.
[17] M. Bagholizadeh, M.B. Hamooleh, A. Alizadeh, A. Torabi, D.J. Jasim, M. Rostamzadeh-Renani, et al., Occupant's thermal comfort augmentation and thermal load reduction in a typical residential building using genetic algorithm, Case Stud. Therm. Eng. 59 (2024) 104491, https://doi.org/10.1016/j.csite.2024.104491.
[18] K. Dhanapal, P. Ragupathy, N. Chinnadurai, Energy efficient machine learning optimization framework for hybrid renewable generation in BIPV systems using DRL–ANN synergy, Sustainable Computing: Informatics and Systems 50 (2026) 101320, https://doi.org/10.1016/j.suscom.2026.101320.
[19] Solar resource maps & GIS data for 200+ countries | Solargis. https://solargis.com/resources/free-maps-and-gis-data, 2026. (Accessed 18 October 2025).
[20] World Climate Regions. https://storymaps.arcgis.com/stories/61a5d4e9494f46c2b520a984b2398f3b, 2026. October 18, 2025.
[21] M. Arslan, M. Çunkaş, An experimental study on determination of optimal tilt and orientation angles in photovoltaic systems, J. Eng. Res. 13 (2025) 2689–2701, https://doi.org/10.1016/j.jer.2024.07.015.
[22] IEC, 63092–1. International Standard: TC 82 Solar photovoltaic energy systems, 2020. IEC 63092–1:2020 | IEC.
[23] IEA, Categorization of BIPV Applications. https://iea-pvps.org/key-topics/categorization-of-bipv-applications/, 2021.
[24] K.S. Anderson, C.W. Hansen, W.F. Holmgren, A.R. Jensen, M.A. Mikofski, A. Driesse, Pvlib python: 2023 project update, J. Open Source Softw. 8 (2023) 5994, https://doi.org/10.21105/joss.05994.
[25] P.G. Loutzenhiser, H. Manz, C. Felsmann, P.A. Strachan, T. Frank, G.M. Maxwell, Empirical validation of models to compute solar irradiance on inclined surfaces for building energy simulation, Sol. Energy 81 (2007) 254–267, https://doi.org/10.1016/j.solener.2006.03.009.
[26] J.E. Hay, J.A. Davies, J.E. Hay, T.K. Won, Calculations of the solar radiation incident on an inclined surface, in: Proceeding of First Canadian Solar Radiation Data Workshop, Ministry of Supply and Services, Canada, 1980. , p. 59.
[27] J.K. Copper, A.B. Sproul, S. Jarnason, Photovoltaic (PV) performance modelling in the absence of onsite measured plane of array irradiance (POA) and module temperature, Renew. Energy 86 (2016) 760–769, https://doi.org/10.1016/j.renene.2015.09.005.
[28] J.A. Duffie, W.A. Beckman, Solar engineering of thermal processes, Wiley, 2013, https://doi.org/10.1002/9781118671603.
[29] S. Jazouli, H.R. Wilson, C. Kapsis, Performance evaluation of predictive models for a grid-connected building-integrated photovoltaic system (BIPV), Energ. Buildings 347 (2025) 116376, https://doi.org/10.1016/j.enbuild.2025.116376.
[30] IEA-PVPS T13, PV Performance Modeling Methods and Practices Results from the 4th PV Performance Modeling Collaborative Workshop, PV Performance Modeling Methods and Practices - IEA-PVPS, 2017.
[31] A. Driesse, P. Jain, S. Harrison, Beyond the curves: Modeling the electrical efficiency of photovoltaic inverters, in: 33rd IEEE Photovolatic specialists conference, IEEE, 2008, pp. 1–6, https://doi.org/10.1109/PVSC.2008.4922827.

[32] M. Wang, C. Wu, P. Zhang, Z. Fan, Z. Yu, Multiscale dynamic correlation analysis of wind-PV Power Station output based on TDIC, IEEE Access 8 (2020) 200695–200704, https://doi.org/10.1109/ACCESS.2020.3035533.

[33] A. Shahin, H.H. Gad, M.E.M. Rizk, W. Hu, S. Abulanwar, Maximum power point tracking using cross-correlation algorithm for PV system, Sustainable Energy, Grids and Networks 34 (2023) 101057, https://doi.org/10.1016/j.segan.2023.101057.

[34] R.P.N.P. Weerasinghe, R.J. Yang, R. Wakefield, E. Too, T. Le, R. Corkish, et al., Economic viability of building integrated photovoltaics: a review of forty-five (45) non-domestic buildings in twelve (12) western countries, Renew. Sust. Energ. Rev. 137 (2021) 110622, https://doi.org/10.1016/j.rser.2020.110622.

[35] P. Corti, P. Bonomo, F. Frontini, P. Mace, E. Bosch, Building Integrated Photovoltaics: A practical handbook for solar buildings' stakeholders, 2020.

[36] E. Saretta, P. Bonomo, F. Frontini, Active BIPV glass facades: current trends of innovation, 2017, pp. 2–7.

[37] CostKu, Construction Engineering Cost Information Network – Material Price and Quotation Database. www.costku.com, 2026 (accessed October 18, 2025).

[38] Ministry of Land, Infrastructure and Transport (MOLIT) 2022, Standard Market Unit Prices for Construction Work: Applicable Work Categories and Unit Prices (2022 Edition), Ministry of Land, Infrastructure and Transport, Sejong, Republic of Korea.

[39] AD-R Reverse Slope Eaves|Alfin Co., Ltd., a manufacturer specializing in eaves. https://www.alfin.co.jp/products/adr/, 2026 accessed October 18, 2025.

[40] What is the price of galvalume steel sheet? Construction unit price and appropriate construction cost | If it's roof repair [Teigak]. https://yanekabeya.com/62056/, 2026. (Accessed 18 October 2025).

[41] Building and Construction Authority (BCA), Standard Schedule of Rates for Building Works, Civil Engineering Works and Electrical Works, Singapore, 2018.

[42] Consol Assoicates, Consol's Nigeria Building Price Book for Builder and Developers, 6th ed, 2022.

[43] Construction Publishers & Consultants, RSMeans Data from Gordian Commercial Renovation Cost Data 32, 2026. United States of America.

[44] Construction price generator, Spain. CYPE Ingenieros, S.A, 2026. https://www.generadordeprecios.info/#gsc.tab=0. accessed October 18, 2025.

[45] Byggnyckeln Kalkyl Grå 2021/2022 | Svensk Byggtjänst. https://byggtjanst.se/bokhandel/bygg-teknik/byggproduktion/byggnyckeln-kalkyl-gra-20212022, 2026. (Accessed 18 October 2025).

[46] Rawlinsons Australian construction handbook. Australia, 2021.

[47] World Population Review, Cost of Electricity by Country 2025. https://worldpopulationreview.com/country-rankings/cost-of-electricity-by-country, 2025 (accessed July 28, 2025).

[48] IEA, Electricity Market Report 2025. https://www.iea.org/reports/electricity-2025, 2025.

[49] E. Vartiainen, G. Masson, C. Breyer, D. Moser, E. Román Medina, Impact of weighted average cost of capital, capital expenditure, and other parameters on future utility-scale PV levelised cost of electricity, Prog. Photovolt. 28 (2020) 439–453, https://doi.org/10.1002/PIP.3189.

[50] H.R. Wilson, F. Frontini, P. Bonomo, G.C. Eder, M. Babin, S. Thorsteinsson, et al., Multi-dimensional evaluation of BIPV installations: development of a tool to assess the performance as building component and electricity generator, Energ. Buildings 312 (2024) 114207, https://doi.org/10.1016/J.ENBUILD.2024.114207.

[51] IEA T15, Building-Integrated Photovoltaics - A Technical Guidebook, Routledge, New York, 2025. Building-Integrated Photovoltaics: A Technical Guidebook - IEA-PVPS.

[52] Q. Yu, K. Dong, Z. Guo, J. Xu, J. Li, H. Tan, et al., Global estimation of building-integrated facade and rooftop photovoltaic potential by integrating 3D building footprint and spatio-temporal datasets 2 (2025) 100060, https://doi.org/10.1016/j.ynexs.2025.100060.

[53] J. López Prol, F. de Llano Paz, A. Calvo-Silvosa, S. Pfenninger, I. Staffell, Wind-solar technological, spatial and temporal complementarities in Europe: a portfolio approach, Energy 292 (2024) 130348, https://doi.org/10.1016/j.energy.2024.130348.

[54] S. Charani Shandiz, B. Rismanchi, G. Foliente, Energy master planning for net-zero emission communities: state of the art and research challenges, Renew. Sust. Energ. Rev. 137 (2021) 110600, https://doi.org/10.1016/j.rser.2020.110600.

[55] S. Sterl, I. Vanderkelen, C.J. Chawanda, D. Russo, R.J. Brecha, A. van Griensven, et al., Smart renewable electricity portfolios in West Africa, Nat. Sustainability 3 (2020) 710–719, https://doi.org/10.1038/s41893-020-0539-0.

[56] G. Glenk, S. Reichelstein, Economics of converting renewable power to hydrogen, Nat. Energy 4 (2019) 216–222, https://doi.org/10.1038/s41560-019-0326-1.

[57] J. Yan, Y. Yang, P. Elia Campana, J. He, City-level analysis of subsidy-free solar photovoltaic electricity price, profits and grid parity in China, Nat. Energy 4 (2019) 709–717, https://doi.org/10.1038/s41560-019-0441-z.

[58] IEA. Best practice guidelines for the use of economic and technical KPIs, PVPS, 2024. https://iea-pvps.org/key-topics/kpi-pvsystems-2024/.

[59] IEA, Uncertainties in Yield Assessments and PV LCOE. https://iea-pvps.org/key-topics/uncertainties-yield-assessments/, 2020.

[60] R. Yang, R. Wakefield, C. Gunarathna, N. Weerasinghe, Cost Reduction and Deployment of Prefabricated Building Integrated Photovoltaics, 2019.

[61] IRENA, Renewable Power Generation Costs in 2024. https://www.pv-tech.org/irena-global-solar-pv-lcoe-increases-by-0-6-in-2024-to-us0-043-kwh/, 2025.

[62] R. Bajo-Buenestado, A.M. Bento, D. Kaffine, Z.E. Marmarelis, Decarbonization and electricity price vulnerability, Nat. Sustainability 8 (2025) 170–181, https://doi.org/10.1038/s41893-024-01502-8.

[63] H. Gholami, H.N. Røstvik, D. Müller-Eie, Holistic economic analysis of building integrated photovoltaics (BIPV) system: case studies evaluation, Energ. Buildings 203 (2019) 109461, https://doi.org/10.1016/J.ENBUILD.2019.109461.